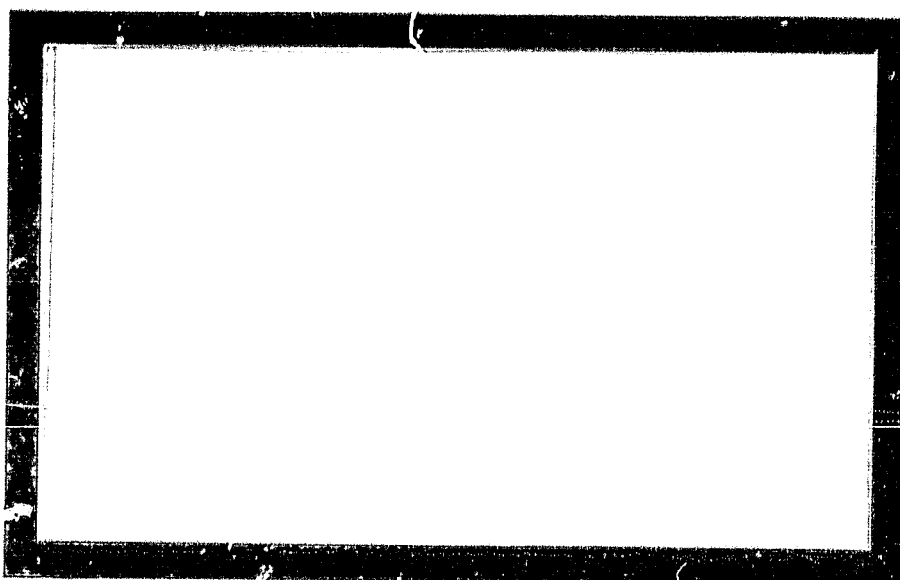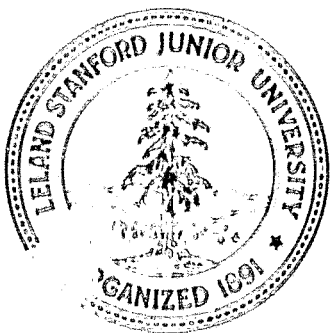# General Disclaimer

One or more of the Following Statements may affect this Document

- This document has been reproduced from the best copy furnished by the organizational source. It is being released in the interest of making available as much information as possible.

- This document may contain data, which exceeds the sheet parameters. It was furnished in this condition by the organizational source and is the best copy available.

- This document may contain tone-on-tone or color graphs, charts and/or pictures, which have been reproduced in black and white.

- This document is paginated as submitted by the original source.

- Portions of this document are not fully legible due to the historical nature of some of the material. However, it is the best reproduction available from the original submission.
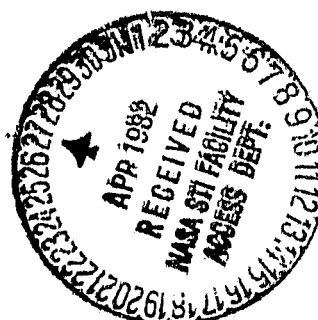
CENTER FOR MATERIALS RESEARCH

STANFORD UNIVERSITY • STANFORD, CALIFORNIA

Center for Materials Research
McCullough Building
Stanford University
Stanford, CA 94305

Final Technical Report
on

DIRECT OBSERVATION OF INTERFACE INSTABILITY

DURING CRYSTAL GROWTH

Contract No. NAS8-33110

Submitted to
National Aeronautics and Space Administration
Washington, D.C.

CMR 82-19
March 1982

Submitted by
The Board of Trustees of
Leland Stanford Jr. University
Stanford, California 94305

Principal Investigator:

Professor W. A. Tiller
Department of Materials Science
and Engineering

Co-Investigators:

Professor R. S. Feigelson
Center for Materials Research

Dr. Dennis Elwell
Center for Materials Research

TABLE OF CONTENTS

I. INTRODUCTION

The general aim of this investigation was to study interface stability and solute segregation phenomena during crystallization of a model system. Emphasis was to be placed on direct observational studies partly because this offered the possibility at a later stage of performing related experiments under substantially convection-free conditions in the space shuttle.

The study originally envisaged was a 4- or 5-year program to obtain a wide range of careful experimental data in order to test the theories of interface stability. This would have necessitated measurements of a large number of material parameters on the system chosen for the investigation, the most difficult being the solute diffusion coefficient in the liquid, the thermal conductivity of the liquid phase and the solid-liquid interfacial energy.

In practice, the program was terminated after 3 years which did not allow time to complete this detailed investigation. It has however, been possible within the 3-year program to make a number of major advances which are important in their own right. The major achievements described in this report are:

1. The development of a new model system for fundamental studies of crystal growth from the melt and the measurement of a range of material parameters necessary for comparison of experiment with theory.

2. The introduction of a new method of measuring segregation coefficient using absorption of a laser beam by the liquid phase.

3. The comparison of segregation in crystals grown by gradient freezing and by pulling from the melt.

4. The introduction into the theory of solute segregation of an interface field term and comparison with experiment.

5. The introduction of the interface field term into the theories of constitutional supercooling and morphological stability and assessment of its importance.

The theoretical part of this investigation is presented first.

II. THEORY

A. Interface Field Effects on Solute Redistribution

Generally, the solute distribution in a crystal has been described in terms of two important parameters, k_0 which is called the equilibrium distribution coefficient or phase diagram distribution coefficient, and k which is called the effective distribution coefficient: k_0 is the ratio of the concentration of solute in the solid, C_S, that that in the liquid, C_L, when equilibrium exists between the two phases at a given temperature, while k is the value of this ratio under the actual conditions of crystallization.

From surface studies, one finds that the chemical potential of a molecule can be quite different in an interface region compared to the bulk phase far from the interface. This is due to differences in local molecular configurations between the two domains arising from (i) gross structural changes in the molecular potential function for an atom situated there rather than in either bulk phase, and (ii) inhomogeneous fields of stress, electrostatic potential, magnetic potential, etc. Therefore, in an interface region, the Gibbs free energy is modified by introducing an "Interface Potential" term through an extended chemical potential

$$\eta^j = \mu^j \quad {}^{\wedge}G^{0j}(x) \tag{1a}$$

$$= \mu^{0j} + \tilde{k}T \, \ell n \, a^j(x) + \Delta G^{0j}(x) \, , \tag{1b}$$

where j refers to the jth solute, a is the activity, μ^o is the standard state chemical potential, $\Delta G^{0j}(x)$ is the interface potential which is the spatial variation of the energy of interaction between the jth solute and all of the interface fields and $\tilde{k}$ is the Boltzmann constant.

In an interface region, the chemical potential difference which comes from differences in local molecular configurations is called the "Interface Potential: and this produces the "Interface Field." The major interface fields of interest are categorized by writing

$$\Delta G^O(x) = f(g(x), \sigma(x), H(x), \phi(x)) . \tag{2}$$

Here $g(x)$ accounts for the variation of local order, local coordination and local density with distance: $\sigma(x)$ accounts for the variation of local stress; $H(x)$ accounts for the variation of local magnetic potential; and $\phi(x)$ accounts for the variation of local electrical potential. At this moment, the formulae of all interface potential terms are not well defined. However, the interface field contribution can be written explicitly [1] as

$$\Delta G^O(x) = Z^j e\phi(x) + \frac{\partial}{\partial C^j} \left[\frac{\varepsilon}{2} (\nabla\phi)^2 + \frac{\sigma^2(x)}{2E^*}\right] + \Delta\mu_{H.M.} + \cdots \tag{3}$$

where Z is the valence, ϕ is the electrostatic potential, ε is the permittivity, σ is the stress, E^* is the elastic modulus, and $\Delta\mu_{H.M.}$ is the chemical potential change relating to different bonding energies for solute versus solvent species in the interface region, and neglected contributions include activity coefficient effects.

In order to evaluate the effect of an interface field on the solute distribution, consider a frame of reference moving at constant velocity V with the interface subject to a nonstirred or a well-stirred fluid at distances greater than $x = \delta$ from the interface and subject to interface interaction energy contributions of the form

$$\delta G_S^O(x) = \beta_S \, \exp(\alpha_S x) \, , \qquad\qquad x < 0 \, , \qquad (4a)$$

$$\delta G_L^O(x) = \beta_L \, \exp(-\alpha_L x) \, , \qquad\qquad x \geq 0 \, . \qquad (4b)$$

This form of field decay has been chosen for its simplicity, where β and α are constants. The overall solute distribution might be represented qualitatively as in Fig. 1 for a stirred fluid. The flux of solute, J is given by

$$\vec{J} = -D\vec{\nabla}C - \frac{DC}{\tilde{k}T} \, \vec{\nabla}\delta G^O(x) - \vec{V}C \, , \qquad (5)$$

in a coordinate system moving with the interface at velocity V. In the steady state,

$$\vec{\nabla} \cdot J = 0 \, , \qquad (6)$$

which has the general solution

$$\nabla C + \left(\frac{\vec{V}}{D} + Be^{\alpha' x}\right)C = \vec{A} \, , \qquad (7)$$

where

$$\text{for solid:} \qquad B = \frac{\alpha_S \beta_S}{\tilde{k}T} : \quad \alpha' = \alpha_S \qquad\qquad (8a)$$

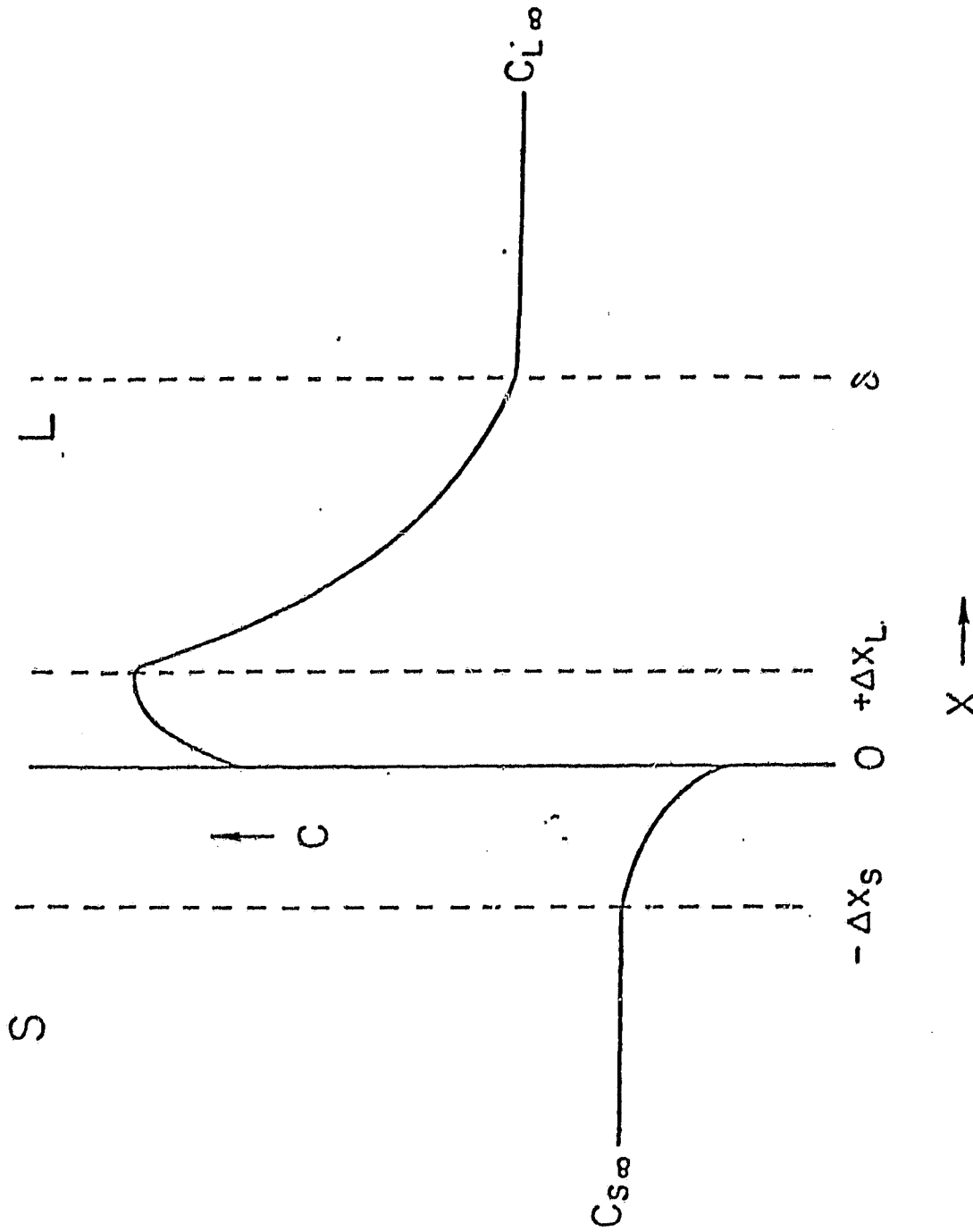$$\text{for liquid:} \qquad B = -\frac{\alpha_L \beta_L}{\tilde{k}T} : \quad \alpha' = \alpha_L \qquad\qquad (8b)$$

Figure 1 Schematic representation of solute distribution in the solid and liquid during freezing from a convectively stirred liquid $(x \gtrsim \delta)$ and with an interface field for the case of $k_o < 1$

Using the integrating factor technique, Eq. (7) has solutions of the form

$$C = E'' \exp\left(-\frac{V}{D} x\right) \exp\left(-\frac{B}{\alpha'} e^{\alpha' x}\right) + A \exp\left(-\frac{V}{D} x\right) \exp\left(-\frac{B}{\alpha'} e^{\alpha' x}\right)$$

$$\times \int^{x} \exp\left(\frac{V}{D} t\right) \exp\left(\frac{B}{\alpha'} e^{\alpha' t}\right) dt \ . \tag{9}$$

Solutions for C_S and C_L are plotted in Fig. 2 as a function of interface position x for a range of growth velocities and with parameters tabulated in the figure. For details of the calculation, see references [1] and [2].

The logarithmic scale is necessary to reveal the two very different scales of phenomena operating in the liquid; i.e., the phase diagram solute partitioning profile and the field-affected interface segregation profile. As a first approximation, we might think of the two as acting independently and Fig. 2 is a direct superposition of the two effects. Thus, the solute-depleted zone at small x for large V indicates a measure of the time response of the solute ahead of the interface to the interface field. At higher velocities, a shorter time exists for such a response so the minumum moves closer to the interface. Only when $V \sim 10^{-2}$ cm/sec does any appreciable pile-up occur at the interface and by $V \sim 10^{-4}$ cm/sec, the equilibrium pile-up is developed. The solute distribution in the solid behaves as expected with the profile extending a few α_S^{-1} and with the solute trapping effect becoming complete at $V \sim 10^{-1}$.

$k_o = 10^{-1}$
$\alpha_S = 10^5$
$\alpha_L = 10^6$
$D_S = 10^{-5}$
$D_L = 10^{-5}$
$\dfrac{\beta_S}{kT} = \dfrac{\beta_L}{kT} = -5$

C_L/C_∞

LIQUID

10^{-4}
10^{-3}
10^{-2}
10^{-1}
$V=1$

C_S/C_∞

SOLID

10^{-4}
10^{-3}
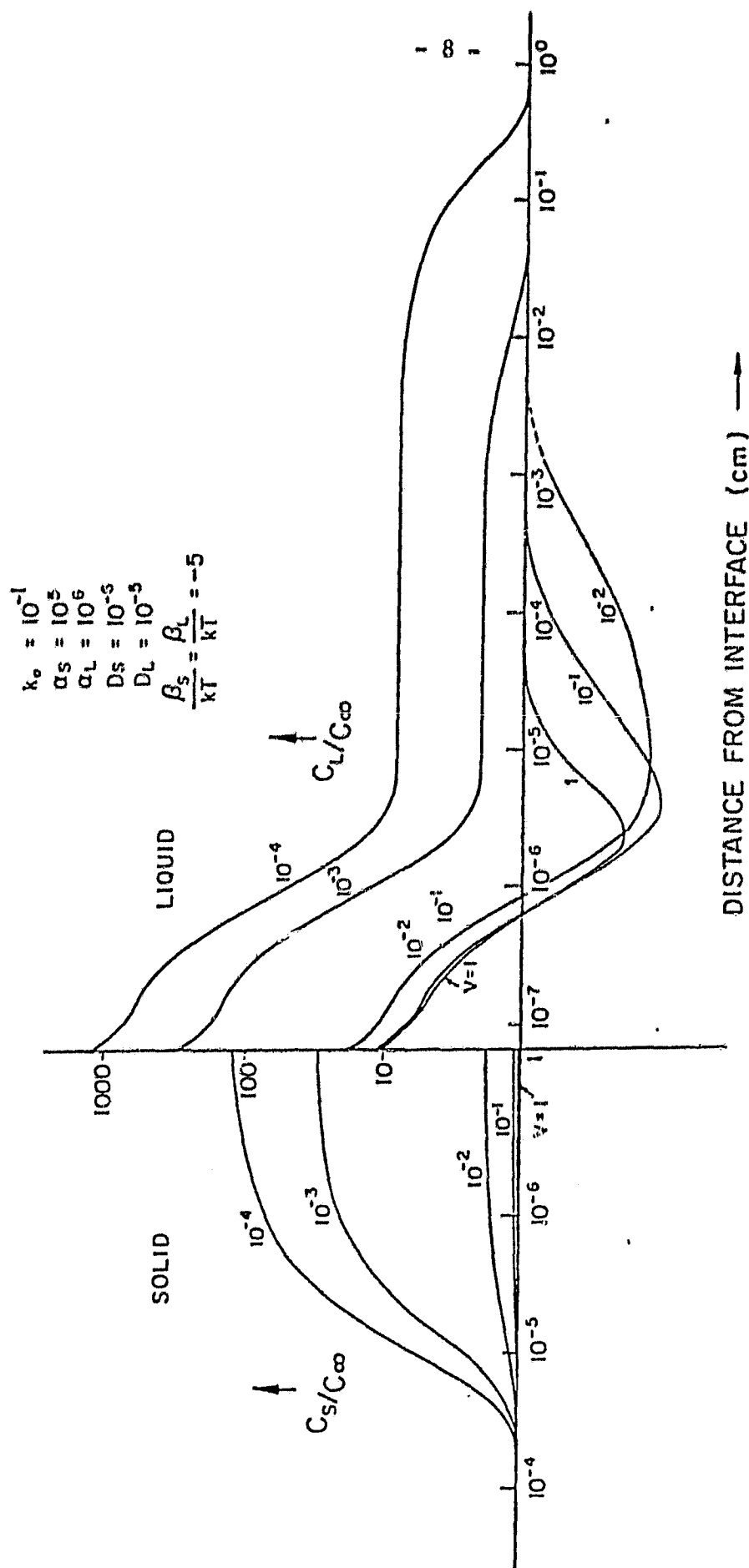10^{-2}

DISTANCE FROM INTERFACE (cm) ——

Figure 2. Computed curves for C_S/C_∞ and C_L/C_∞ as a function of interface position for several interface velocities $V = 10^{-4}$, 10^{-3}, 10^{-2}, 10^{-1}, 1 cm/sec and the fixed parameters noted on the figure

We seek an expression for the effective distribution coefficient, k, given by

$$k = C_{S'}-\Delta X_S)/C_L(\infty) \quad . \tag{10}$$

for a stirred melt such that $C_L = C_L(\infty)$ as $x \to \delta$. The solution [1,2] is of the form

$$k = \frac{k_i}{k_i+[(\frac{V}{\alpha_S D_S})(-\frac{\tilde{k}T}{\beta_S})^{V/(\alpha_S D_S)} \exp\{\frac{(\beta_L-\beta_S)}{\tilde{k}T}\}\gamma_S+k_1(\frac{V}{\alpha_L D_L})(-\frac{\tilde{k}T}{\beta_L})^{V/(\alpha_L D_L)}\gamma_L]\exp\{-\frac{V\delta}{D_L}\}} \tag{11a}$$

and an approximate summation for the gamma function γ_S gives

$$k = \frac{k_i}{k_i + [\exp\{\frac{(\beta_L-\beta_S)}{\tilde{k}T}\} <1+\tilde{\gamma}_S> - k_1(-\frac{V}{\alpha_L D_L})(-\frac{\tilde{k}T}{\beta_L})^{-V/(\alpha_L D_L)}\gamma_L] \exp\{-\frac{V}{D_L}\delta\}} \tag{11b}$$

In the limit as β_S and $\beta_L \to 0$, $\tilde{\gamma}_S \to 0$,

$$(-\frac{V}{\alpha_L D_L})(-\frac{\tilde{k}T}{\beta_L})^{-V/(\alpha_L D_L)}\gamma_L + 1 \quad ,$$

and $k_i \to k_0$. Thus, we have

$$k = \frac{k_0}{k_0 + (1-k_0)\, e^{-V\delta/D_L}} \tag{12}$$

which is the familiar BPS result [3] for no interface field effects. In Eq. (11), k_i is the interface distribution coefficient $C_S(0)/C_L(0)$ which can be obtained in terms of k_o by putting $\eta_S = \eta_L$ (see Eq. (1)). An alternative form of Eq. (11b) is

$$k = \frac{k_o}{k'_o + \{(1+\tilde{\gamma}_S) - k'_o(-\frac{V}{\alpha_L D_L})(-\frac{\tilde{k}T}{\beta_L})^{-V/(\alpha_L D_L)}\gamma_L\} \exp\{-\frac{V\delta}{D_L}\}} \quad , \quad (13)$$

where $k'_o = k_0[\gamma_S(\infty)/\gamma_S(0)]\ [\gamma_L(\infty)/\gamma_L(0)]^{-1}$.

To illustrate the effect of β, α and D changes on k, we first explored the range $-5 < (\tilde{\beta}/kT) < 5$, $10^2 < \alpha_L < 10^6$, $10^{-7} < V < 0^{-1}$ with $D_S = 10^{-8}$, $D_L = 10^{-5}$, $k'_0 = 10^{-1}$, $\delta = 10^{-1}$ and $10^2 < \alpha_S < 10^7$. If $k'_o/\alpha_L D_L \ll 1/\alpha_S D_S$, and β_S effects are dominant over the β_L effects and vice versa if $k'_o/\alpha_L D_L \gg 1/\alpha_S D_S$. As expected. for $\beta_S < 0$, $\kappa(\tilde{\beta}/kT) > k(0)$ while for $\beta_S > 0$, $k(\tilde{\beta}/kT) < k(0)$. This effect is illustrated in Fig. 3, which plots $k(5)$, $k(0)$ and $k(-5)$ as a function of V for $\beta_L = 0$, $\alpha_S = 10^6$ and $\alpha_L = 10^2$. Only a small difference occurs between $k(-5)$ and $k(0)$. Usually, $k \to k'_o$ as $V \to 10^{-7}$ cm/sec for all β_S and α_S and $k \to 1$ as $V \to 10^{-3} - 10^{-2}$ cm/sec.

There does not appear to be any suitable data with which to quantitatively compare our theoretical results primarily because so much parameter information is needed to meaningfully test Eq. (13). Only with this objective in mind would investigators gather and record all the needed data for an adequate test. However, it is useful to project how one would go through such a comparison with experimental data and we shall do this with Hall's data on germanium [4]. To test Eq. (13), we would plot $\ln (1/k - 1)$ versus δ for fixed V and versus V for fixed δ. In the former case this should be a linear plot with slope V/D_L and intercept
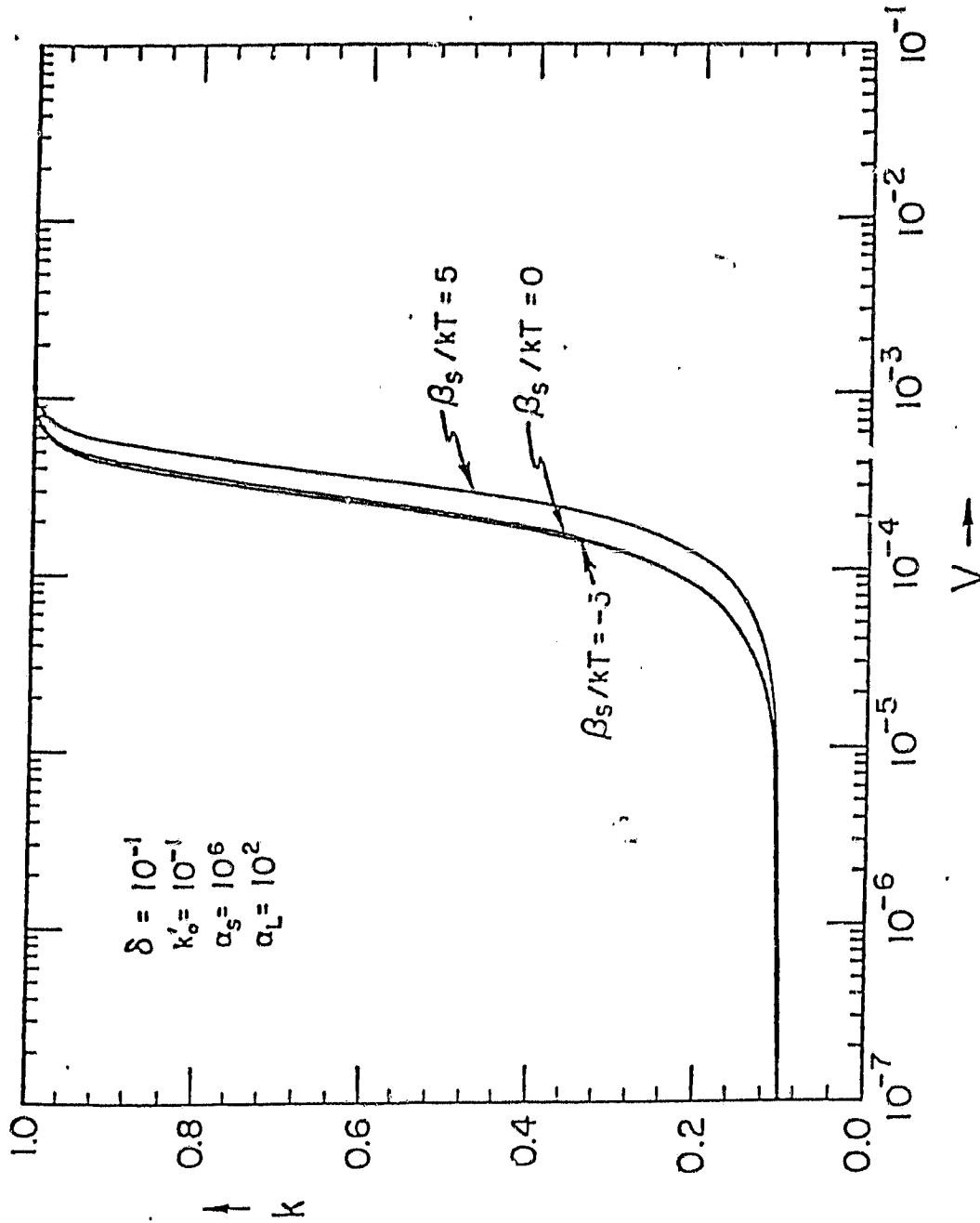
Figure 3: Calculated plots of effective distribution coefficient, k, as a function of V for three values of $\beta_S/\tilde{k}T$ and $\beta_L/\tilde{k}T = 0$ ($D_S = 10^{-8}$; $D_L = 10^{-5}$ cm^2/sec)

$$\ell n\Big[\frac{(1+\tilde{\gamma}_S)}{k'_o} + \Big(\frac{V}{\alpha_L D_L}\Big)\Big(-\frac{\tilde{kT}}{\beta_L}\Big)^{-V/(\alpha_L D_L)}\gamma_L\Big] \quad . \tag{14}$$

This intercept should vary with V and the magnitude of the variation will indicate the magnitude of the field effect. In the latter case a nonlinear plot should obtain for a nonzero field effect and the greater the degree of nonlinearity, the greater the magnitude of the field effect.

The simplifying assumption for Ge or Si systems is that, because the liquid is metallic, we can approximate $\beta_L \sim 0$ so that

$$\ell n\Big(\frac{1}{k} - 1\Big) = \ell n\Big(\frac{1+\tilde{\gamma}_S}{k'_o} - 1\Big) - \frac{V\delta}{D} \quad . \tag{15}$$

In addition, assuming that k'_o is approximately independent of V,

$$\frac{d}{dV}\Big[\ell n\Big(\frac{1}{k} - 1\Big)\Big]_{V\to 0} = -\frac{\delta}{D_L} + \Big(\frac{1}{1-k'_o}\Big)\Big(\frac{d\tilde{\gamma}_S}{dV}\Big)_{V\to 0}$$

$$= -\frac{\delta}{D_L} + \Big(\frac{1}{1-k'_o}\Big)\sum_{n=1}^{\infty}\Big[\frac{(\beta_S/\tilde{kT})^n}{\alpha_S D_S^n \, n!}\Big] \tag{16a}$$

$$= -\frac{\delta}{D_L} + \frac{(\beta_S/\tilde{kT})(1/\alpha_S D_S)k'_o}{(1-k'_o)} \quad , \quad \text{for } \Big|\beta_S/\tilde{kT}\Big| \ll 1 \tag{16b}$$

so that the initial slope yields a value for β_S/α_S through its departure from the zero interface field value of $-\delta/D_L$. Finally, as $V \to \infty$, $d\tilde{\gamma}_S/dV \to 0$ and

$$\frac{[d \, \ell n\big(\frac{1}{k} - 1\big)]}{dV} = -\frac{\delta}{D_L} \quad . \tag{16c}$$

Replotting Hall's data in this fashion, as in Fig. 4, we find that $d \ln(1/k - 1)/dV$ seems to approach a constant slope at large V. From this value, we obtain $\delta/D_L \sim 57$ sec/cm and this yields a value of $D_L \sim 2.4 \times 10^{-5}$ cm^2/sec for Sb in Ge. From the $V = 1$ inch/hr intercept, we obtain $k'_0 \approx 2.2 \times 10^{-3}$ compared to a tabulated value [5] of $k_0 = 3.0 \times 10^{-3}$. From the slope at $V = 0$ (same value as $V = 1$ in/hr), which is -428 sec/cm, we obtain $(\beta_S/kT)(1/\alpha_S D_S) \approx -1.7 \times 10^5$ sec/cm by assuming that $|\beta_S/kT| \ll 1$. From Fig. 4 at $V = 9$ in/hr, we require that $\ln((1+\tilde{\gamma}_S-k'_0)/k'_0)$ be ≈ 5 so that $\tilde{\gamma}_S \approx -0.67$. This leads to $\alpha_S = 9.2 \times 10^6$ cm^{-1} ($D_S = 5 \times 10^{-10}$ cm^2/sec) [6] and $\beta_S/kT \approx -1.17$ for the (100) face, which violates our initial assumption of $|\beta_S/kT| \ll 1$. A more correct analysis yields values of $\beta_S/kT \approx -1.7$ and $\alpha_S D_S \approx 2.62 \times 10^{-3}$ cm/sec for the (100).

The values of β_S/kT for the various crystal faces differ by ~ 0.1 with the (111) having the largest magnitude. The sign of the binding energy indicates an Sb buildup at the interface probably due to a negative electrostatic potential binding of Sb$^+$ ion cores to the interface region.

If β_L is not neglected, it should be possible to separate the effects of interface fields in the solid and liquid phases but it was difficult to find the most suitable values for β_S, β_L, $\alpha_S D_S$ and $\alpha_L D_L$ using the data and computer facilities available.
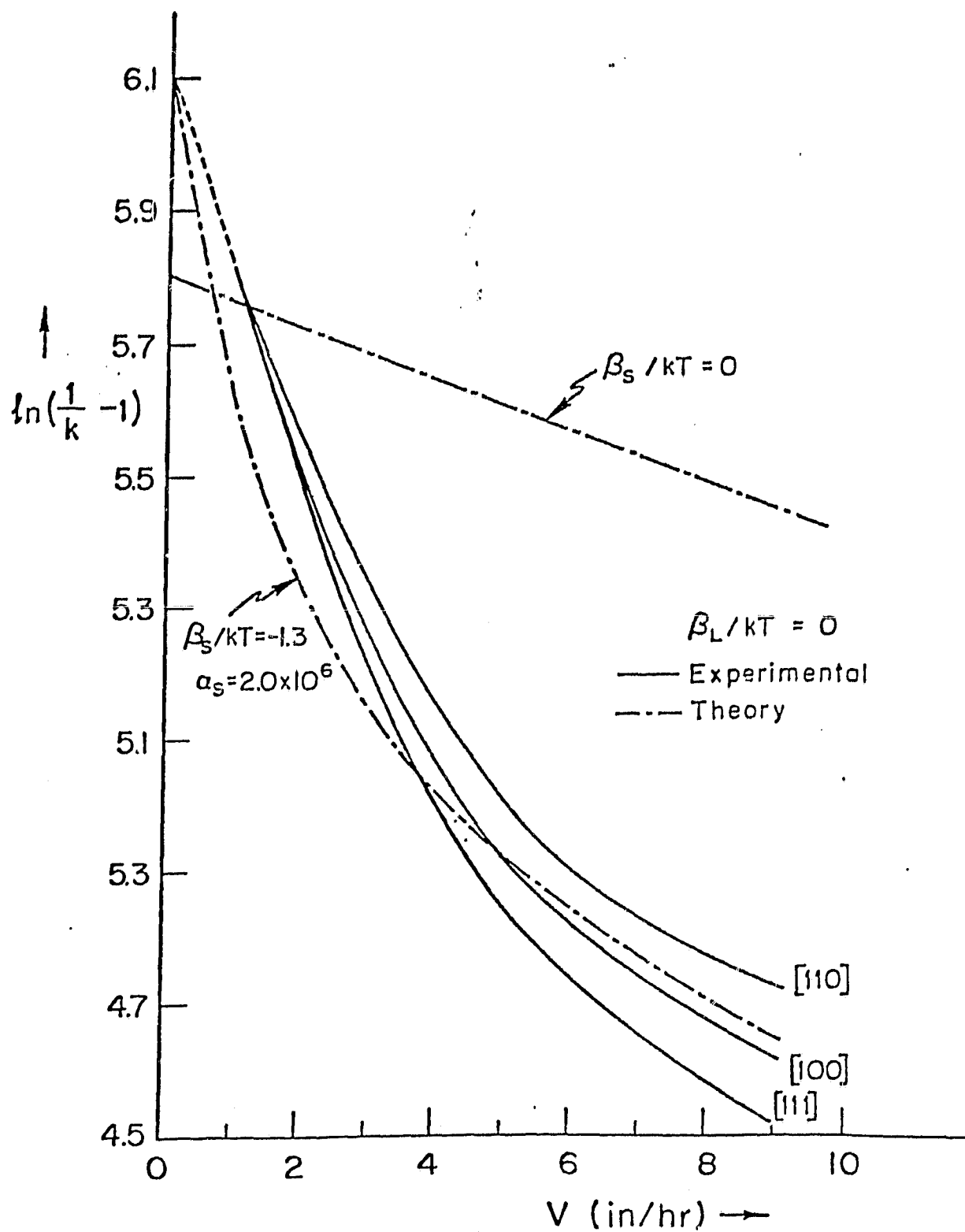
Figure 4: Comparison of theory with experiment using Hall's data

B. Interface Field Effects on Constitutional Supercooling

Generally, the constitutional supercooling criterion (CSC) may be written as

$$\left(\frac{dT_L}{dx}\right)_{x=0} > \left(\frac{dT_A}{dx}\right)_{x=0} \quad , \tag{17}$$

where T_L is the liquidus temperature and T_A is the actual temperature. For the steady state growth situation with no interface field present, this CSC becomes

$$\frac{G_L}{V} < \frac{|M_L|(1-k_o)C_\infty}{D_L k_o} \quad . \tag{18}$$

Thus far, this CSC has been based on a static analysis, provided that interface attachment kinetics are infinitely fast and the interfacial free energy is negligible. However, when we have an interface field present, Eq. (18) is no longer valid and we must modify the liquidus slope M_L to M_L^* which includes the interface field effect:

$$M_L^* = M_L \exp(\delta G_L^o/RT) \quad , \tag{19}$$

where $\delta G_L^o = (\Delta G_L^{o2} - C\Delta G_L^{o1})$, and superscripts 1 and 2 refer to solvent and solute, $C = v^{o2}/v^{o1}$ is the volume ratio for the liquid phase and v^o is the specific volume.

Using the same interface field representation defined above, and noting that $C_i = C_S/k_i$, we find [2,7] that

$$\frac{(dT/dx)_i}{V} \leq \frac{-M_L^*}{D_L} \, C_\infty \left\{ \frac{\exp\left(-\frac{\beta_L}{\tilde{k}T}\right)}{k'_o} \left[1 - \frac{D_L}{V} \frac{\alpha_L \beta_L}{\tilde{k}T}\right] \left[1 + \sum_{n=1}^{\infty} \frac{(\beta_S/\tilde{k}T)^n}{(1+\frac{\alpha_S D_S n}{V})n!}\right] - 1 \right\} \tag{20}$$

For the case of metallic liquids, $\beta_L \approx 0$ and α is large so we probably need to keep the $\alpha_L \beta_L$ term in Eq. (20) even though we may be justified in setting $\exp(-\beta_L/kT) \approx 1$. For $\beta_S = 0$, this would tend to reduce the r.h.s. of Eq. (20) and thus decrease the tendency toward constitutional supercooling. Depending on the sign and magnitude of β_S, the tendency can be either further decreased or increased. For the case of germanium discussed earlier, since $\tilde{\beta}_S/kT \approx -1.3$ and $k_o' \approx 0.73 k_o$, w expect that, for $\beta_L = 0$, the r.h.s. of Eq. (20) will be decreased below that of Eq. (18) so that the interface should be stable even in the presence of some constitutional supercooling as evaluated using the old criterion. Estimates of the size of this effect for $CsCdCl_3$ under various assumed values for β_S and β_L (see Section VI) are shown in Fig. 5.

C. Interface field Effects in the Morphological Stability Analysis

An alternative and elegant approach to the planar interface instability criterion was developed by Mullins and Sekerka in 1964 and independency by Voronkov [9]. This treats the time-dependence of an infinitesimal distortion of a plane interface. If it grows, it causes a permanent shape change and leads to an unstable interface state: whereas, if it shrinks, it leads to a stable interface state. Mullins and Sekerka assumed a sinusoidal disturbance of amplitude δ and calculated the conditions under which $\dot{\delta}$ (= $d\delta/dt$) was positive.

We consider the solute redistribution for both solid and liquid in a frame of reference moving at constant velocity V_X with the interface subject to a nonstirred liquid and subject to an interface interaction energy contribution of the form
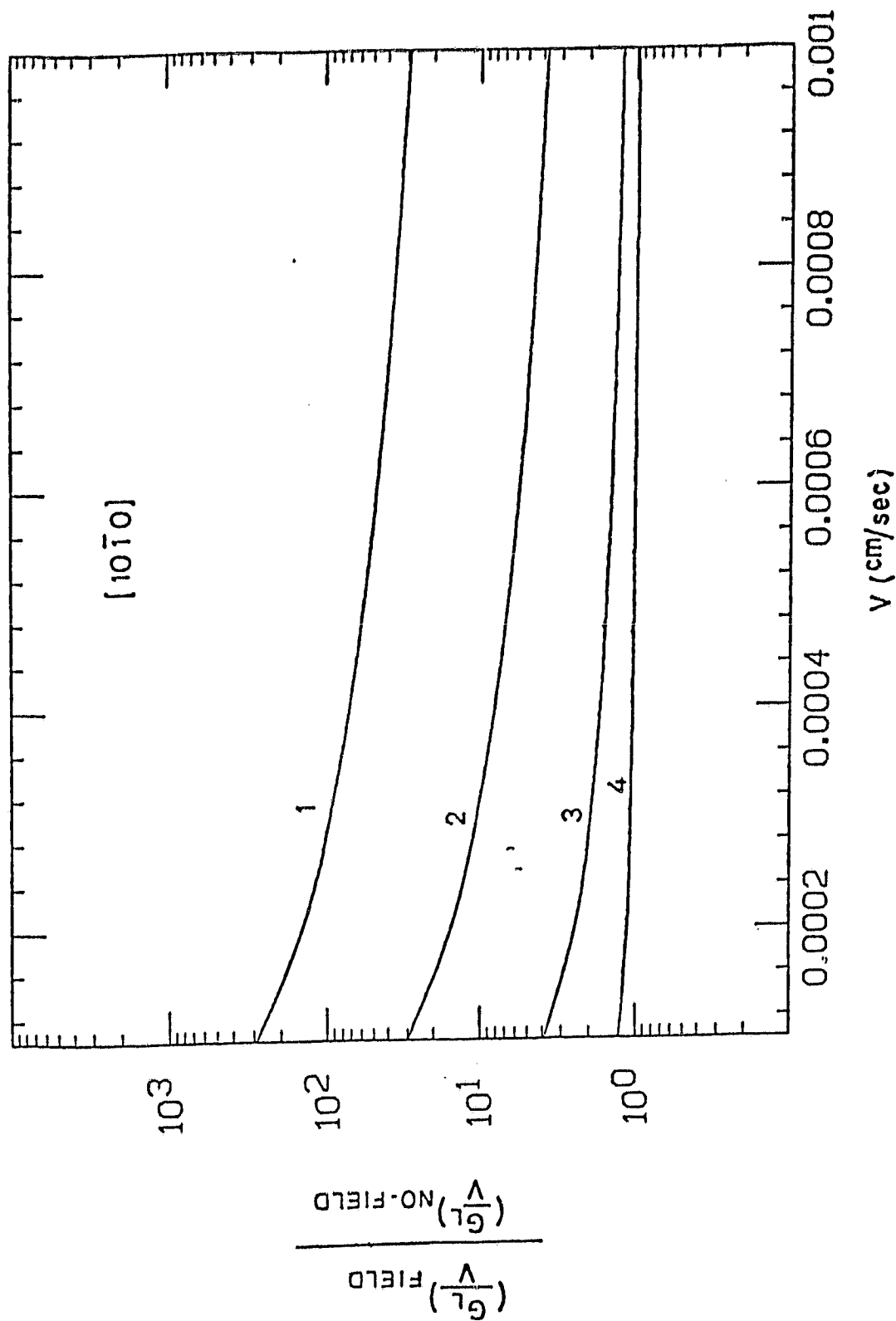
Figure 5 : Calculated plots of $(G_L/V)_{field}/(G_L/V)_{no-field}$ versus V illustrating the importance of $\beta_S/\tilde{k}T$ and $\beta_L/\tilde{k}T$ for the Co $-$ CsCdCl$_3$ system ($\alpha_L = 1.4 \times 10^5$/cm, $D_L = 7.38 \times 10^{-6}$ cm^2/sec, $k'_o = 0.115$) (3.2b) $\beta_S/\tilde{k}T = -0.25$, $\alpha_S D_S = 4 \times 10^{-3}$ cm/sec, (1) $\beta_L/\tilde{k}T = 10^{-1} \times \beta_S/\tilde{k}T$, (2) $\beta_L/\tilde{k}T = 10^{-2} \times \beta_S/\tilde{k}T$, (3) $\beta_L/\tilde{k}T = 10^{-3} \times \beta_S/\tilde{k}T$, (4) $\beta_L/\tilde{k}T = 10^{-4} \times \beta_S/\tilde{k}T$

$$\delta G_S^o(\gamma) = \beta_S \, \exp(\alpha_S r) \quad , \qquad r \leq 0 \tag{21a}$$

$$\delta G_L^o(\gamma) = \beta_L \, \exp(\alpha_L r) \quad , \qquad r \geq 0 \tag{21b}$$

where β and α are constants and subject to a sinusoidal shape perturbation with an amplitude δ and wavelength λ.

The governing equation for solute transport is

$$\vec{J}_{solute} = -D[\vec{\nabla}C + \frac{C}{\tilde{k}T} \, \vec{\nabla}(\delta G^o) + \frac{V_x}{D} \, C] \tag{22a}$$

where D is the diffusion coefficient of solute, which is assumed constant. The governing equation for heat transport is

$$\vec{J}_{thermal} = -D_t(\vec{\nabla}T + \frac{V_x}{D_t} \, T) \tag{22b}$$

where D_t is thermal diffusivity which is also assumed to be constant.

A steady state condition will be assumed and this requires that, $\partial C/\partial t = -\vec{\nabla} \cdot \vec{\nabla} J_{solute} = 0$ and $\partial T/\partial t = -\vec{\nabla} \cdot \vec{\nabla} J_{thermal} = 0$. For the definition of δG^o and only taking the first order δ terms into consideration

$$\vec{\nabla}(\delta G^o) = (\frac{\partial}{\partial X} \vec{i} + \frac{\partial}{\partial Z} \vec{k}) \, (\delta G^o)$$

$$\tilde{=} \alpha\beta \, e^{\alpha X}\{\vec{i}(1 - \alpha\delta \cos \omega Z) + \vec{k}(\omega\delta \sin \omega Z)\} \, , \tag{23a}$$

and

$$\vec{\nabla} \cdot \vec{\nabla}(\Delta^o G) \tilde{=} \alpha\beta \, e^{\alpha X}\{\alpha + \omega^2 - \alpha^2)\delta \cos \omega Z\} \, . \tag{23b}$$

Unfortunately, using these formulae, we cannot solve analytically the governing equation of solute transport which has the ultimate form of

$$\nabla^2 C + \frac{\vec{\nabla}(\delta G^o)}{\tilde{k}T} \cdot \vec{\nabla}C + \frac{C}{\tilde{k}T} \vec{\nabla} \cdot \vec{\nabla}(\delta G^o) + \frac{V_X}{D} \cdot \frac{\partial C}{\partial X} = 0 \ . \tag{24}$$

However, once we specify a certain system, we can solve the above equation by numerical analysis methods.

To solve the solute transport equation analytically, we assume that the interface interaction energy has a linear form such as

$$\delta G^o = \beta(1 + \alpha r_n) \ , \tag{25}$$

and this holds only within $|r_n| < |1/\alpha|$. Then, we can write

$$\vec{\nabla}(\delta G^o) \stackrel{\sim}{=} \beta\alpha(\vec{i} + \vec{k} \ \delta\omega \sin \omega Z) \ . \tag{26a}$$

$$\vec{\nabla} \cdot \vec{\nabla}(\delta G^o) \stackrel{\sim}{=} \beta\alpha\delta\omega^2 \cos \omega Z \ , \tag{26b}$$

and we have the general solution to Eq. (24), which is

$$C_1 = A_0 + A_1 \exp[-(\frac{P_o}{kT} + \frac{V_X}{D})X] + (A_2 \ e^{-\omega^* x} + A_3 \ e^{-\omega^{**} x}) \cos \omega Z \ . \tag{27}$$

If we obtain a similar solution for $|x| > |1/\alpha|$ and apply continuity equations for C and J at $x = |1/\alpha|$, we can obtain concentration and temperature distribution. After much tedious algebra [2,7], the stability relation becomes

$$\left(\frac{\dot{\delta}}{\delta}\right)_{A-T} = \left(\frac{1}{\Delta H}\right) \left[\left(\frac{L\ L}{D_{Lt}} - \frac{S\ S}{D_{St}}\right)V_X - \omega(K_S G_S^* + K_L G_L^*)\right.$$

$$\left. + \omega(K_S + K_L) \left\{M^*(Q_{L1}+1)A_{L3} - T_M \Gamma \omega^2 - M^* \frac{C_\infty(\frac{V_X}{D_L})\ (NUM)}{(DEN)}\right\}\right] . \qquad (28)$$

where (NUM) and (DEN) are complex functions of D_S, α_S, V etc. To
illustrate the interface field effect on $\dot{\delta}/\delta$, we will identify the Mullins
and Sekerka result as $(\dot{\delta}/\delta)_{M-S}$ and ours as $(\dot{\delta}/\delta)_{A-T}$. We first explore
the range $-3 < \tilde{\beta}_S/kT < 3$ and $-3 < \tilde{\beta}_L/kT < -1 \times 10^{-4}$ for 10^{-4} cm/sec $<$
$V_X < 1$ cm/sec with $\alpha_S = \alpha_L = 10^6$, and $\omega = 10^4$ for the ice-water-KCl
system. We used all the experimental values for the ice-water-KCl system
quoted by Kotler [10] except for the surface energy which is $\gamma = 29.1$ mJ/m^2
from Trivedi [11]. The values used are $\Delta H = 80$ cal/g, $T_M = 273°K$,
$K_S = 4K_L = 5.3 \times 10^{-3}$ cal/(cm/sec - °C), $k_0\ 5 \times 10^{-4}$,
$M_L = 1.7°C/(mole-liter^{-1})$, $C_\infty = 0.01$ mole/liter, $D_L = 5 \times 10^{-5}$ cm^2/sec,
$D_S = 10^{-8}$ cm^2/sec, and $G_L = 25°C/cm$. From Fig. 6 we can observe the very
marked difference between the two criteria. This difference is not easily
explainable by using a single special instability mechanism but it should be
obvious that the interface field effects influencing the constitutional
supercooling criterion, and the point effect on the lateral diffusion, are
two major contributions of this very large difference between $(\dot{\delta}/\delta)_{A-T}$ and
$(\dot{\delta}/\delta)_{M-S}$. From Fig. 6, we can especially note that only a small $\tilde{\beta}_L/kT$
value is needed to generate a large effect. Therefore, dealing with a
material system which obviously manifests an interface field (electrostatic),
but neglecting the field effect on the stability criterion as people have in
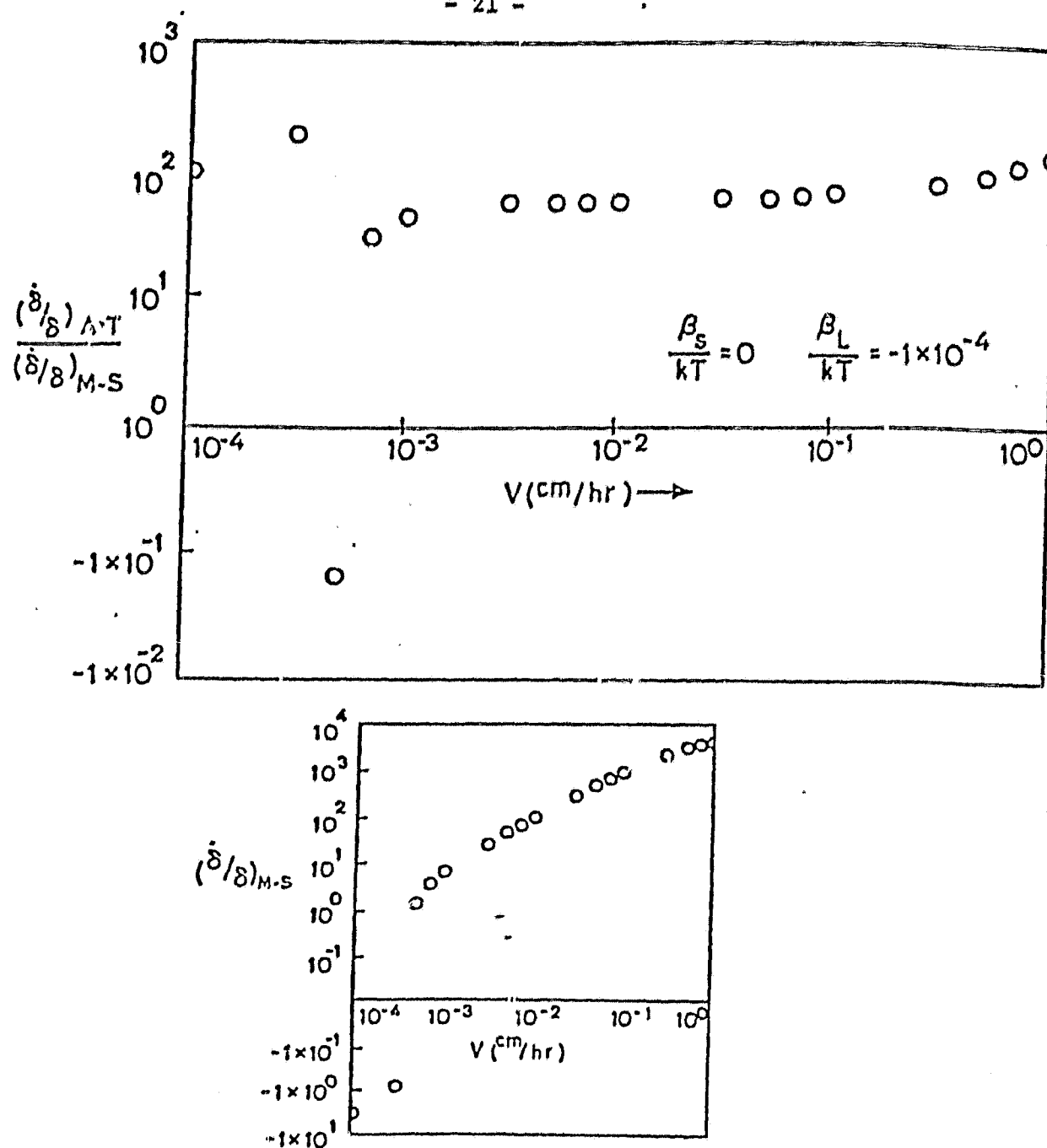the past, produces a markedly erroneous result.

Figure 6: Calculated plots of $(\dot{\delta}/\delta)_{A-T}/(\dot{\delta}/\delta)_{M-S}$ versus V illustrating the importance of $\beta_S/\tilde{k}T$ and $\beta_L/\tilde{k}T$ for Ice-Water-KCl system, and calculated plot of $(\dot{\delta}/\delta)_{M-S}$ versus V for this system $(\beta_S/\tilde{k}T = 0,\ \beta_L/\tilde{k}T = -1 \times 10^{-4})$

III. CHOICE OF MATERIAL FOR EXPERIMENTAL STUDY

The material requirements sought were that crystal growth should be possible by the Czochralski method and by gradient freezing, that transparent crystals could be grown without major problems and that the melting point should be sufficiently low to permit direct observation of the growing crystals. In addition, it was necessary to find a suitable dopant of fairly low phase diagram distribution coefficient for quantitative studies of solute partitioning during Czochralski growth. These requirements were met by cesium codmium chloride, $CsCdCl_3$ and a preliminary report on the favorable properties of this material for crystalization studies has been published [12].

A. Phase Diagram

The phase diagram [13] for $CsCl - CdCl_2$ (Fig. 7) shows three compounds: $CsCdCl_3$ which melts congruently at $553°C$, Cs_2CdCl_3 with a congruent melting point of $488°C$ and Cs_3CdCl_5 which melts incongruently at $390°C$. It has been confirmed by DTA that $CsCdCl_3$ melts congruently with no phase transitions between the melting point and room temperature but the melting point of purified material is actually $545°C$.

Investigation of the crystal structure of $CsCdCl_3$ has confirmed that it is hexagonal with $a = 7.418$ Å and $c = 18.39$ Å as reported by Siegel and Gebert [14] rather than monoclinic as given by Naray-Szabo [15] and Belyaev, et al. [13] or cubic perovskite as reported by Marsh and Savage [16]. Molten $CsCdCl_3$ has appreciable volatility and a quartz crucible, 42 mm in diameter and containing about 160g of material at its melting point, was found to lose between 0.3 and 2.6 wt%/day depending on its
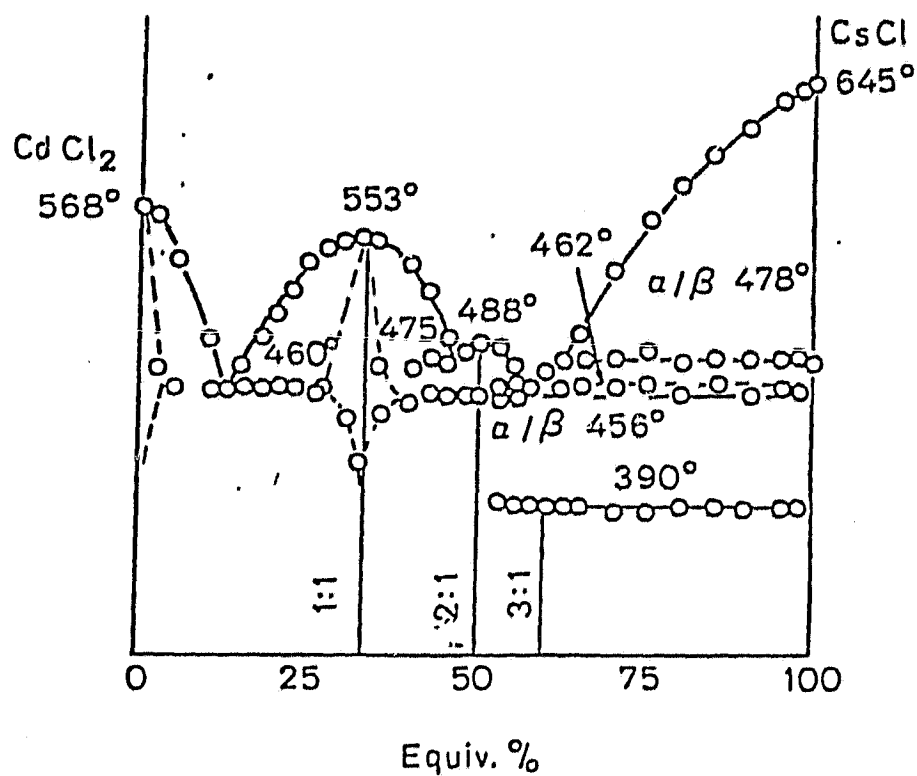
Figure 7:   Phase diagram of CsCl - CdCl$_2$ system [33]

deviations from stoichiometry (when we used the materials as received from vendors). The $CdCl_2$-rich material of highest volatility in this range had a melting point of 535°C and lost $CdCl_2$ by evaporation, but the stoichiometric material was found to evaporate congurently. The solubility of $CsCsCl_3$ in water is reported as 53.7 g/ℓ at room temperature [16]. Although this rather high solubility suggests that powdered material will be hygroscopic, the rate of attack by atmospheric moisture of the surface of crystals was found to be very slow and no signficant handling problems were encountered.

The source materials used were CsCl of 99.95% purity (Harshaw) and "ultra pure" $CdCl_2 \cdot 2H_2O$ (Alfa Ventron). The cadmium chloride hydrate was dehydrated first by a very slow vacuum treatment at room temperature to prevent hydrolysis $(CdCl_2 + 2H_2 \rightarrow Cd(OH)_2 + 2HCl)$ and then by heating in vacuum at 200°C for 24 hours. The dehydrated $CdCl_2$ was purified by zone refining or distillation (vapor transport). Both purification methods were applied to CsCl but the vacuum distillation gave higher purity material and was, therefore, used in a majority of the experiments. Major impurities in the distilled material were 1 ppm Ca and 0.4 ppm Si.

Problems were encountered in zone refining CsCl because of the stress generated at the solid-liquid interface during the 2nd pass which frequently led to fracture of the silica tube. This problem was alleviated but not eliminated by coating the inside of the tube with pyrolytic graphite. Vacuum distilled $CdCl_2$ contained 3 ppm of Ca, 1 ppm of Al and < 1 ppm of Mn and Si. Some experiments were performed using a commercial source of high purity anhydrous CsCl and $CdCl_2$ (Metalsmart). Impurities reported for these materials were 2 ppm Si and 0.5 ppm Cu and Mn in the

$CdCl_2$ and 4 ppm Ba and Rb, and 1 ppm each of Al, Ca, Cu, K, Mg, Na and Si in the CsCl.

B. Solute (Dopant)

$CsCdCl_3$ can be doped for solute redistribution studies by replacing $CdCl_2$ with a divalent transition metal chloride. $CoCl_2$ produces a blue coloration, $CuCl_2$ an orange-brown and $NiCl_2$ a pink. It is assumed that the transition metals enter the lattice as divalent ions but this has not been confirmed. All these impurities exhibit a low segregation coefficient but quantitative data are not available except for Co. The rate of back-diffusion of copper ions during cooling of the crystal may be very fast, depending on the orientation. Therefore Cu is not a suitable dopant for this study. Absorption spectra of doped crystals in the visible and near UV regions shows, in each case, strong absorption at short wavelengths (approximately 3000 Å). In the case of the Cu-doped crystal, a broad absorption band extended to about 5000 Å, with no other peaks in the visible range. The Co-doped and Ni-doped crystals had peaks centered at 6200 Å and 5000 Å respectively. Since the absorption peak of Co-doped $CsCdCl_3$ includes the 6328 Å emission line of the He-Ne laser and cobalt does not exhibit appreciable back-diffusion, this dopant has been used for this study.

C. Property measurements

We attempted to measure all the experimental parameters for the $CsCdCl_3$ system needed to compare the theory with the experimental results for interface instability of $CsCd_{1-x}Co_xCl_3$. Most of the parameters were

found successfully; however, insurmountable difficulties were found in measuring the thermal diffusivity. The parameters that were successfully measured are listed below.

1. Liquidus slope measurement

The slope of the liquidus curve was measured on a Dupont Differential Scanning Calorimeter (DSC). Great care was necessary in sample preparation in order to eliminate moisture and to produce homogeneous samples of known composition. Because of the high degree of supercooling encountered with this material, the liquidus temperature data were taken during heating of the sample from the onset of melting. The results are shown in Fig. 8.

2. Specific heat Cp

The specific heat of $CsCdCl_3$ was also measured by using the Dupont DSC, with sapphire as reference. The specific heat was found to be approximately 0.45 Jg^{-1} deg^{-1} around room temperature, 0.33 Jg^{-1} deg^{-1} just below the melting point, and 0.30 ± 0.01 Jg^{-1} deg^{-1} in the temperature range from 580 to 620°C.

3. Latent heat of fusion ΔHf

The latent heat of fusion of undoped $CsCdCl_3$ was measured by the DSC and found to be 132 J/g. This experiment was done simultaneously with the luquidus slope measurement. The latent heat of fusion of $CsCd_{1-x}Co_xCl_3$ showed a slight increase with Co concentration.

PHASE DIAGRAM OF $C_s Cd_{1-x} Co_x Cl_3$

SYSTEM

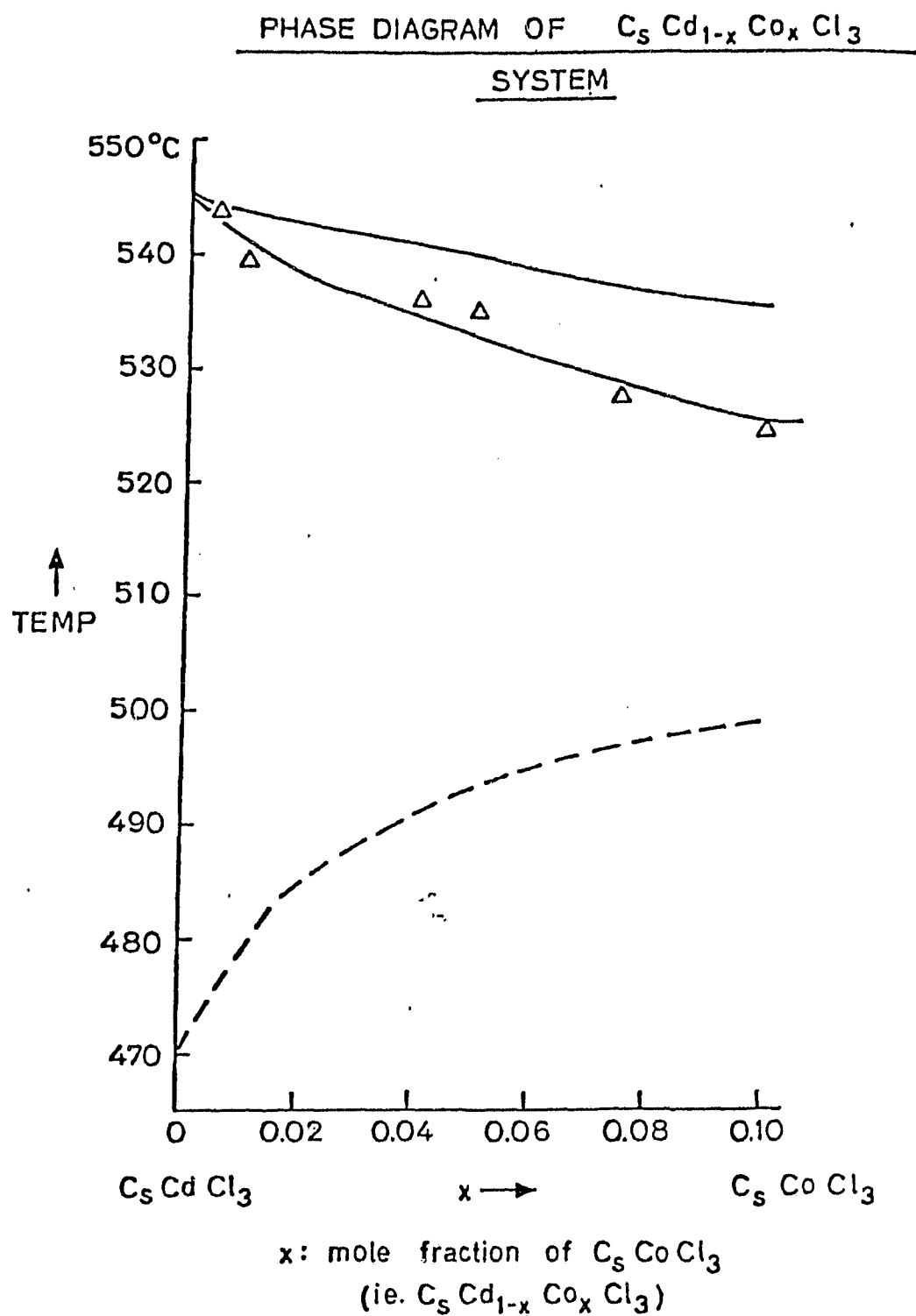x: mole fraction of $C_s Co Cl_3$
(ie. $C_s Cd_{1-x} Co_x Cl_3$)

Figure 8: Liquidus slope measurement of $CsCd_{1-x}CoCl_3$ system

4. Density ρ

The density of molten $CsCdCl_3$ was measured by a direct method using a cathetometer to measure the height of an isothermal column of liquid. The density was found to be 3.03 g/cm^3 at 564 ± 4°C. The error of measurement of the density is about 2%.

The density of solid $CsCdCl_3$ was determined at room temperature by an Archimedean method. The value obtained was 4.03 g/cm^3. It was found that the $CsCdCl_3$ expands 24.7% of its volume when it melts, which is rather large in comparison with most molten salts.

5. Viscosity η

The viscosity of molten $CsCdCl_3$ was found to be too low for the falling sphere method, so an inclined tube technique [17] was used. Using water at room temperature as a standard, the viscosity measured using bronze spheres was found to be η = 1.35 cp just above the melting point.

6. Thermal diffusivity D_t

We tried to measure the thermal conductivity of liquid and solid $CsCdCl_3$ using a "semi-infinite plate" method with periodic temperature variations. The liquid (or solid) specimen is contained in a double crucible with a relatively thin layer of material between the upper and lower crucibles. A periodically varying heat source supplied heat to one surface and the temperature was measured by axial thermocouples welded to the two metallic surfaces which enclosed the sample. The apparatus was calibrated against standard material which was sodium nitrate. However,

when we experimented with $CsCdCl_3$ in Ni crucibles, it severely attacked the crucibles and we could not find suitable crucibles for $CsCdCl_3$.

The apparatus was reconstructed using silver, but $CsCdCl_3$ vapor was found to attack the heating element very rapidly once the temperature was raised above the melting point. Time was not available to build a modified version with a protected element, and attempts to locate a laboratory with the capability to undertake this measurement were unsuccessful.

Table 1 lists the measured parameters for $CsCdCl_3$.

Table 1

Measured Parameters of $CsCdCl_3$

M   Liquidus slope   6/°C/wt%

Cp   Specific heat   0.45 J/g-°C at R.T.   0.30 ± 0.01 J/g-°C at 600°C

ΔH   Heat of fusion   132 J/g

ρ   Density   4.3 g/cm^3 (solid)   3.03 g/cm^3 at M.P. (liquid)

μ   Viscosity   1.35 cp at M.P.

IV. STUDIES OF INTERFACE SHAPE AND STABILITY

Studies of cobalt-segregation and the onset of interface instability have been made using the apparatus shown in Fig. 8. A 2-zone furnace was wound on a grooved ceramic tube which had few vertical slots 7 cm long to allow illumination and observation of the growing crystal. The temperature gradient was controlled by two independent temperature controllers, and crystal growth was achieved by programmed cooling of the upper zone.

Theories of solute distribution and interface stability normally apply to a plane interface and so attempts were made to achieve a fairly planar solid-liquid interface over a wide range of values of g, the fraction of metal solidified. The general principles which determine the interface shape are well established [18]. If the interface is to be planar, the heat flux from the liquid must be the same as heat through the solid; if the crucible receives a net heat flux from the exterior, the interface will tend to be convex and if it radiates heat to the surroundings the interface will be concave. Solution of the heat-transfer equation has been given a sample of infinite length [19] but only a very approximate solution is possible for a finite length. In practice it is found difficult to maintain a heat interface as growth proceeds [19] and typical interface shapes at various stages of growth in unseeded and [0001] seeded cases are shown in Fig. 9. This shows typical trends in the development of the interface shape of $CsCdCl_3$ with time as growth proceeds at slow speed ($\lesssim$ 1 mm/hr) in a temperature gradient of $22°C$ cm^{-1} in samples containing a low concentration of cobalt ($\sim$ 0.005 a/o Co replacing Cd). The interface is normally slightly convex (as seen from the liquid) and the convexity tends to decrease as solifification approaches 100%. In the case of the
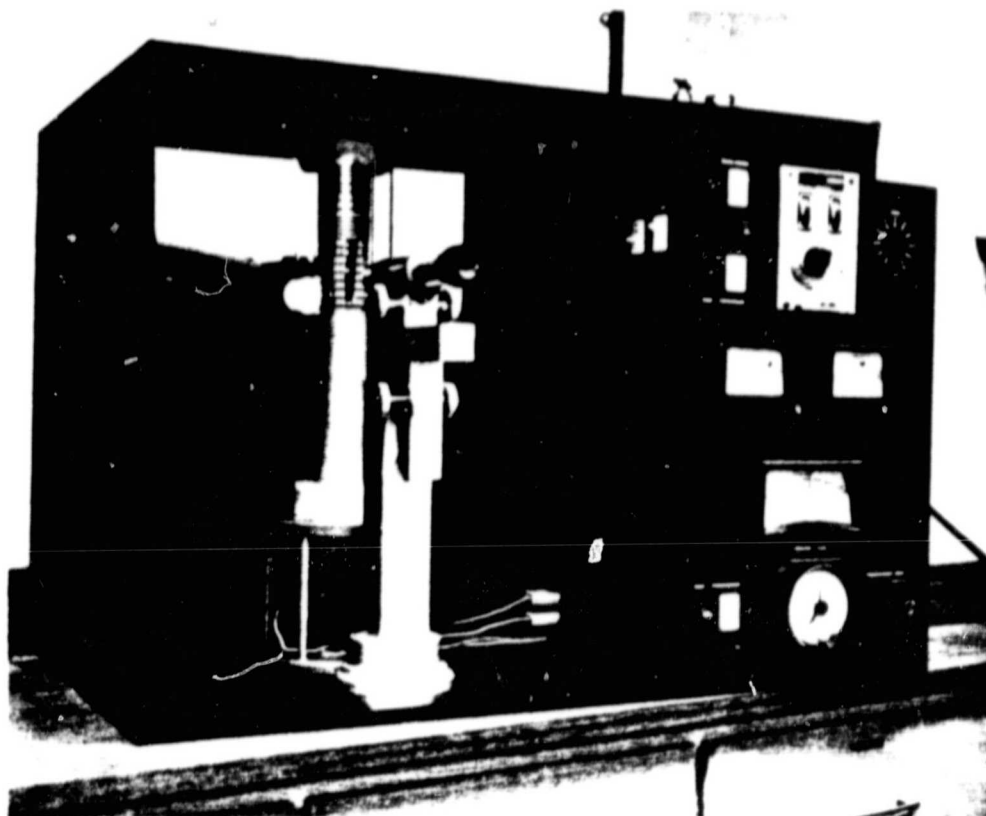
Figure 9 . General view of furnace and
controls.

seeded growth (Fig. 9b) the convexity passes through a maximum in the region where the axial temperature gradient in the liquid is a minimum as suggested by growth rate data. The convex interface shape suggests that $K_s/K_1 > 1$, although this has not yet been confirmed by direct measurement.

Our observations have shown that the convexity of the interface decreases as the furnace temperature gradient is increased. In the furnace used to date, the maximum temperature gradient is $22.2°C$ cm^{-1}, and this was found to be adequate to give a substantially flat interface over a wide range of growth conditions. Reducing the gradient to approximately $14°C$ cm^{-1} caused pronounced convexity of the interface under similar conditions. The dependence of interface shape on growth speed was relatively minor, flatter interfaces being observed as the cooling rate was increased to the range where the interface shape became unstable and cellular growth occurred.

The most striking observation in our preliminary experiments was the occurrence of a marked dome shape as the cobalt concentration was increased from 0.005 to 0.01 a/o (see Fig. 10). At such a low concentration the cobalt cannot be expected to cause a strong change in any of the crystal or melt properties. However, the cobalt does cause a very noticeable increase in the coloration of the melt and therefore in the absorption coefficient over a range of visible and presumably infrared wavelengths, and this increased absorption increases as the crystal grows and cobalt is rejected into the liquid by the normal segregation mechanism. The occurrence of a markedly convex interface as the heat flow through the liquid phase is decreased is entirely consistent with theory: a diminished axial flow is
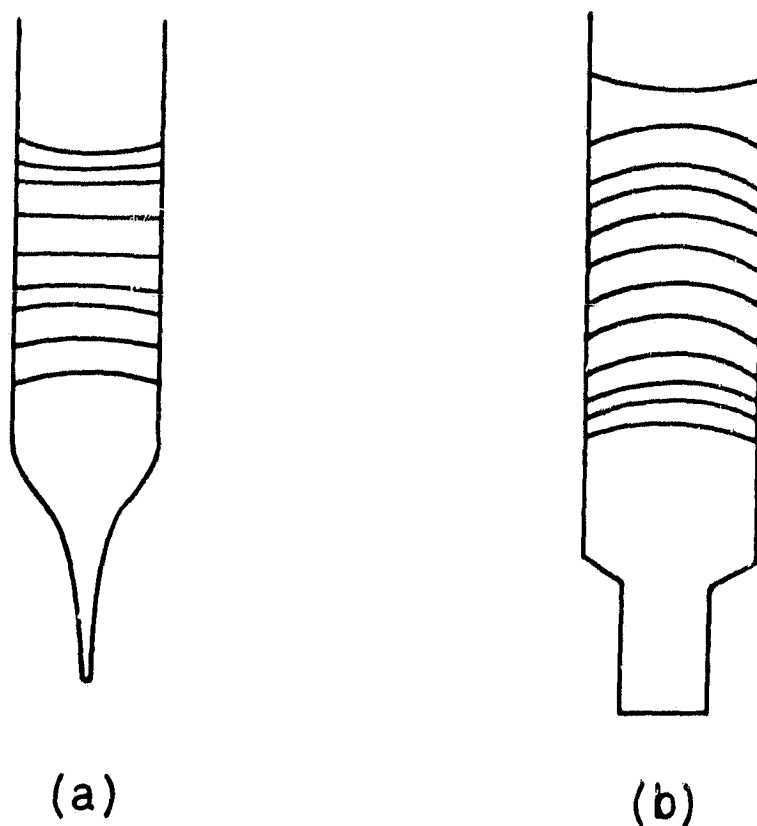
(a)   (b)

Figure 10(a):   Variation in interface shape of $CsCdCl_3$ as
                growth proceeds at slow speed in a temperature
                gradient of 22.2°C/cm in samples of low cobalt
                concentration (~.005 at % Co replacing Cd)
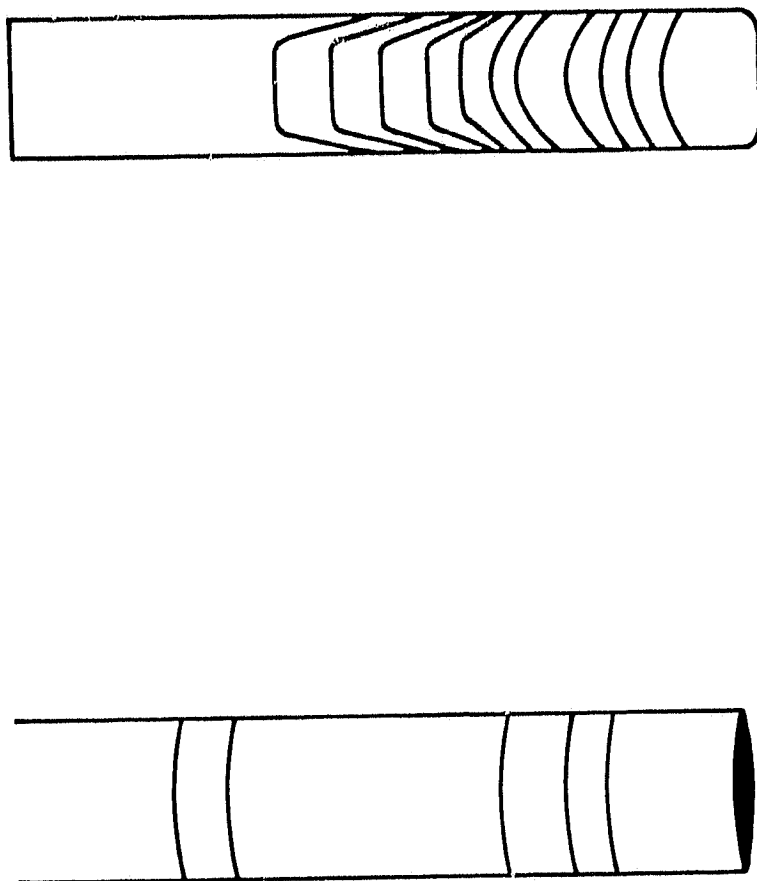   (a) unseeded growth (b) [0001] seeded growth.

Figure 10(b): Change in interface shape of $CsCdCl_3$ when Co concentration is raised from 0.005 (left-hand figure) to 0.01 (right-hand figure).

compensated by increased radial flow of heat into the sample under conditions where the flow through the solid remains constant, so that the convexity increases.

It was reasoned that decreasing the axial heat flow through the crystal would oppose this effect and therefore restore a more nearly planar interface. An experiment was therefore performed in which the bottom surface of the capsule was coated with a gold film to reflect infrared (and visible) radiation transmitted through the crystal. In contrast to our predictions, the presence of this gold coating caused an even steeper convex interface, and the crystal grew with a liquid boundary groove separating it from the capsule along its whole length (see Fig. 11). The reason for this effect is not understood, although conduction of heat through the silica crucible may be an important effect in maintaining a relatively high temperature at the walls.

The growth rate during growth at constant cooling rate was found to vary signficantly during the growth of a crystal typically 5 ± 1 cm in length. Typical data is shown in Fig. 12. In the steady state, the growth rate V is given by

$$V = \theta/G \qquad (29)$$

where θ is the cooling rate and G the temperature gradient. Although this equation is not expected to apply to a relatively short crystal, a maximum in the growth rate is to be expected since G will increase at both ends of the sample due to radiation from the hot zone and to the cold zone of the furnace respectively. In addition, the steeper decrease in V
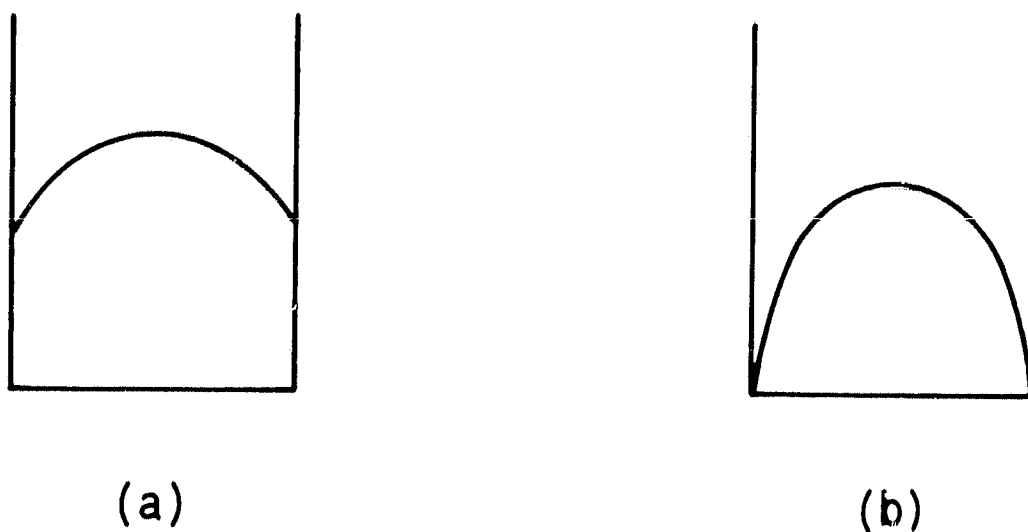
(a)   (b)

Figure 11:   Change in interface shape of $CsCd_{0.99}Co_{0.01}Cl_3$
at same stage of growth (a) original condi-
tions, see right hand figure of Figure 10(b);
(b) with a gold coating across bottom of
crucible.   In this latter case the crystal
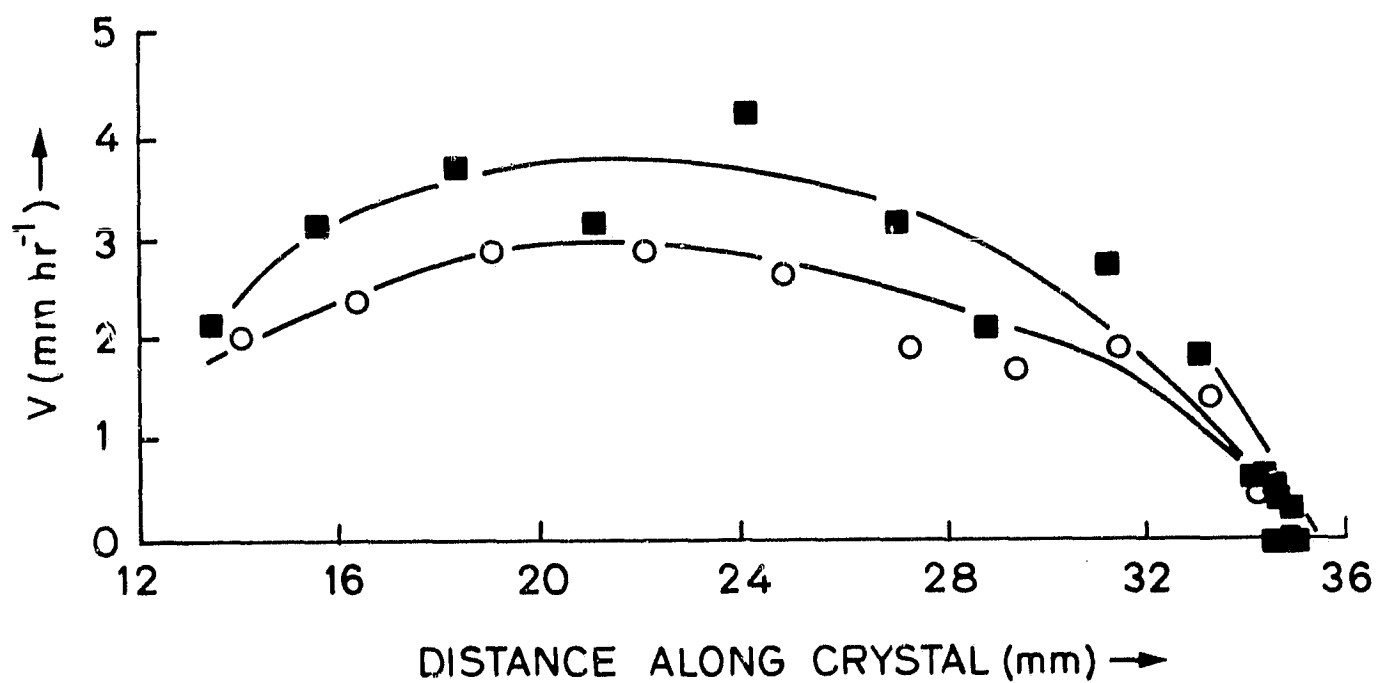grew surrounded by a groove containing liquid.

Figure 12: Variation of growth rate of CsCdCl$_3$ crystals with position during growth by gradient freezing. Temperature gradient: 17.9°C/cm; 0 22.2°C/cm.

FIG 12

during the final stages of solification is due to the build-up of cobalt concentration ahead of the interface, with corresponding decrease in liquidus temperature.

No attempt was made to explain quantitatively the variation of the growth rate as solification proceeded. Both this and especially the changes in interface shape are considered worthy of more detailed investigation, which would involve measurements of the temperature profile within the melt. The influence of heat absorption in the liquid phase as the cobalt concentration increased is of particular interest.

Table 2 summarizes our initial investigation which was aimed at identifying the critical growth rate for the onset of instability and its dependence on the temperature gradient to which the sample was subjected. The same [0001] seeded sample was used in each case, with the cobalt concentration maintained constant at $x = .0025$. The results showed a general tendency for the maximum stable growth rate to increase with the temperature gradient, as expected. The "approximate growth rate" values quoted in the table are unreliable as they include the region where growth slows signficantly towards the end of the solification. If we take the critical cooling rate in each case and assume Eq. (29) for the growth rate, the maximum stable growth rate is 2.2 mm/hr for a gradient of 22.2°C/cm, 1.4 mm/hr for a gradient of 17.9°C/cm and 1.0 mm/hr for 14.3°C/cm. Hence $V_{max} \propto G$, approximately, in agreement with theory.

These early studies showed, however, the need for continuous monitoring of the interface position in order to obain an accurate value for the growth rate at the instant of breakdown. It was found to be difficult to determine precisely the moment where growth became unstable, even on film.

Table 2

Summary of Obsrvations of [0001] Crystal

A. Temperature Gradient 22.2°C/cm

Cooling Rate (°C/hr)	Approximate Growth Rate mm/hr	Range of Measurement (mm)	Observations
0.8	0.65	8-22	Stable
2.5	0.9	31-34	Stable
4.0	1.6	14-37	Perhaps temporary instability
4.5	1.3	19-32	In verge of instability
4.75	1.4	23-34	On verge of instability
5.0	1.8	19-35	Slight instability

B. Temperature Gradient 17.9°C/cm

1.0	0.5	9.30	Stable
2.0	1.0	15-35	Stable
2.25	1.0	24-35	Stable
2.5	1.2	23-32	Slight instability
4.5	1.8	26-32	Unstable

C. Temperature Gradient 14.3°C/cm

0.66	0.6	16-24	Stable
1.0	0.7	24-31	Stable
1.25	0.7	20-32	Stable
1.5	1.0	20-27	Unstable
2.0	1.0	15-18	Unstable

More careful observations suggested that the above values for V_{max} were low by a factor of 2. In addition, the validity of the results at the lower gradient was affected by the curvature of the interface which became pronounced when values below 22°C/cm were used.

Since the constitutional supercooling criterion is of the form

$$\frac{G}{V} < \frac{mk(1-k_o)C}{D_L k_o} = \frac{m(1-k_o)C_\infty}{D_L k_o} \tag{18}$$

a test of it's validity requires measurement not only of G and V_{max} but also of C_∞ (in addition to m, k_o and D_L in separate experiments). In all previous experiments of which we are aware, C_∞ has never been measured directly during the course of a crystal growth experiment but has been inferred from later measurements of the dopant concentration C_S in the crystal. Emphasis was therefore given to the development of a method for the determination of the concentration C_L of cobalt in liquid CsCdCl$_3$ since this concentration can then be measured on a continuous basis. The same method can be used for measurement of the distribution coefficient k, including (by extrapolation) the equilibrium value k_o.

Refinement of our filming technique continued in order to improve the visibility of the onset of interface breakdown, and seed crystals which would completey fill an 8 mm I.D., fused silica tube of square cross section were introduced. The use of high magnification confirmed that, when the interface does become unstable, it breaks down into the cellular structure predicted by morphological stability theory [8]. An example is shown in Fig. 13.
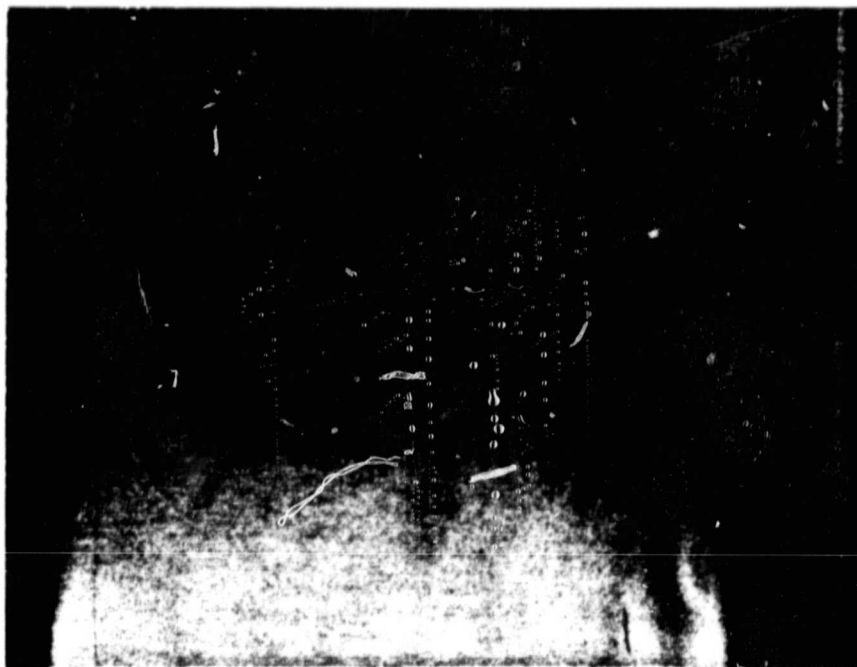
Figure 13:   Solid-liquid interface during crystal growth of
               $CsCdCl_3$ showing onset of cellular growth. The
               periodicity of the cellular structure is about
               200 um.

V. MEASUREMENT OF DISTRIBUTION COEFFICIENT USING LASER LIGHT ABSORPTION

It was mentioned in Section III.B that cobalt-doping of $CsCdCl_3$ intro-duces a broad absorption peak centered at 6200Å and that this peak includes the 6328Å emission line of a He-Ne laser. This suggested that the absorp-tion of a He-Ne laser beam could be used as the basis of Co determination in molten (or solid) $CsCdCl_3$ and an arrangement was set up using a Hughes 10 mW laser (Model 322SH-PC) and a detector (Model SD-4444111261) from Silicon Detector Corp. The output from the detector used in a photovoltaic mode was found to depend very strongly on the cobalt concentration.

The absorption was calibrated using molten $Cs\,Cd_{1-x}\,Co_x\,Cl_3$ samples of known values of x, and the absorption coefficient α was found to depend linearly on the Co concentration. The voltage registered by the dectector was around 5V for $x = 0$ and fell to ~ 1 mV for $x = 0.004$. The measurement is therefore very sensitive within this region but the signal-to-noise ratio fell below the useful range for $x > .004$.

A minor disadvantage of the laser absorption method is that the absorption coefficient for the He-Ne laser light is temperature-dependent. Since this dependence was found to be significant, the calibration was carried out at a temperature just above the melting point. A second calibration was obtained at ~ 630°C, which decreases the apparent value of α by 10%. This decrease is attributed to broadening of the absorption peak due to motion in the fluid.

In order to obtain accurate values of distribution coefficient, it was found to be necessary to measure the length of both the liquid and solid column using a cathetometer. The ratio of these two quantities gives g, the volume fraction of material solidified.

The absorption coefficient in the liquid just ahead of the interface was used to give a colbalt concentration C_L as a function of g. According to the normal freezing equation,

$$C_L = S_o(1-g)^{k-1} \quad , \tag{30}$$

where S_o is the amount of solute in the liquid at the onset of growth and k is the effective segregation coefficient. Our data was therefore plotted as graphs of $\ln C_L$ versus $\ln(1-g)$ which have a slope of $-|k-1|$. A computer least squares fit was used to find the value of k for different values of the growth rate V. Sample data were shown in the report for November 1981.

Data over a side range of values of the growth rate were obtained for both $\langle 0001 \rangle$ and $\langle 34\bar{7}3 \rangle$ orientations. The latter was not chosen deliberately but measurements were made on a crystal which grew after a $\langle 0001 \rangle$ seed had melted due to a sudden increase in temperature.

Figure 14 is a summary of the experimental data in the form of plots of $\ln(k^{-1}-1)$ versus growth rate V for the two orientations. This form of extrapolation is suggested by the BPS equation [3]

$$k = \frac{k_o}{k_o + (1-k_o) \exp(-V\delta/D_L)} \quad , \tag{12}$$

where k_o is expected to be the equilibrium value of the distribution coefficient. Although Eq. (12) is not expected to apply exactly to gradient freeze growth but fits the data within the experimental error. The values obtained are $k_o = .02(7)$ for $\langle 0001 \rangle$ and $k_o = .07(4)$ for $\langle 34\bar{7}3 \rangle$. The estimated error is $\pm .02$ for $\langle 0001 \rangle$ and $\pm .03$ for $\langle 34\bar{7}3 \rangle$ so
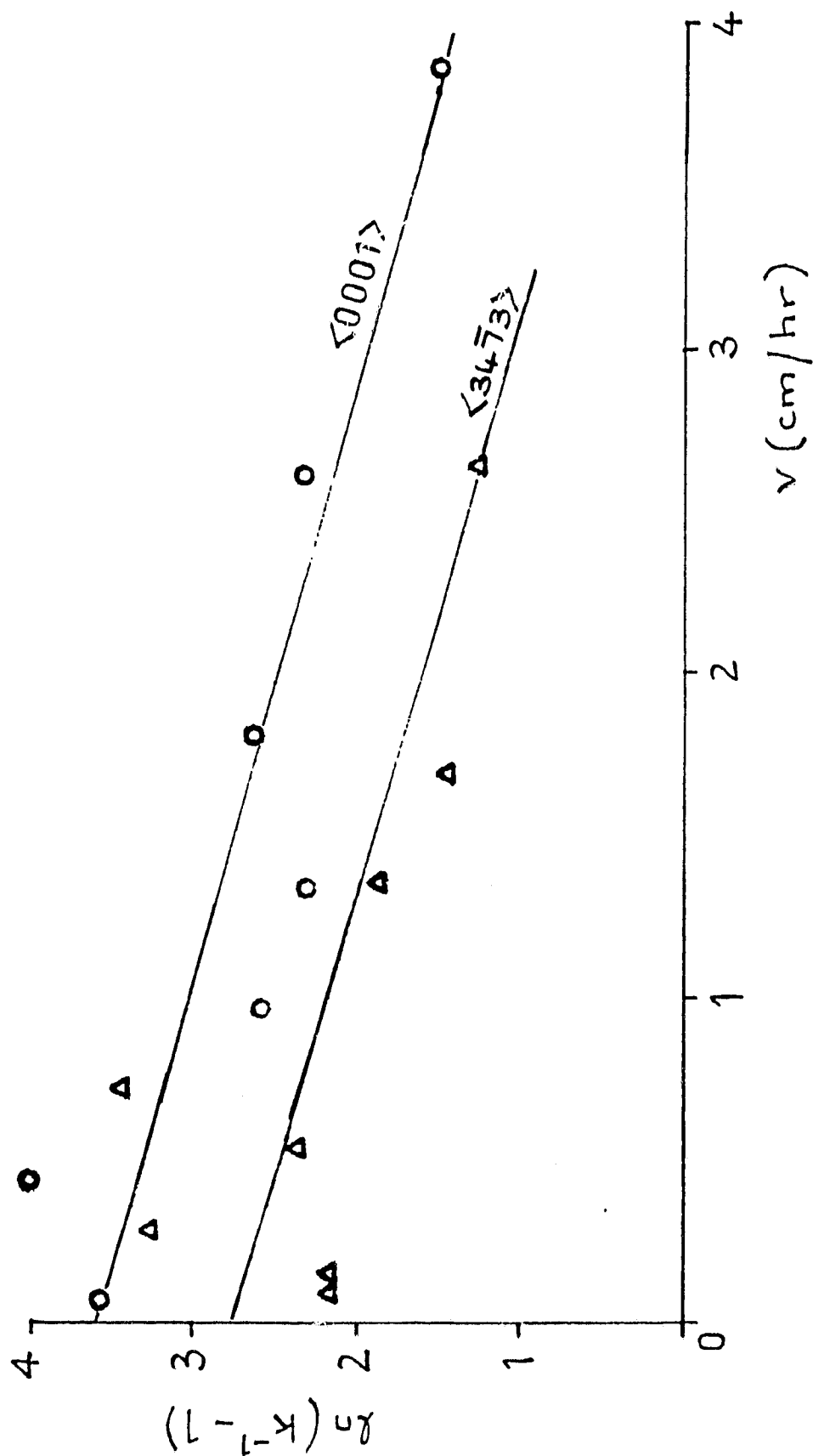
Figure 14: Log of $(K^{-1}-1)$ versus growth rate V for cobalt in CsCdCl$_3$ for two orientations (gradient freeze growth).

the difference between the two directions is just outside the estimated limits.

The slope of the least squares fit is 2.0×10^3 s cm^{-1} for $\langle 0001 \rangle$ and 2.1×10^3 s cm^{-1} for $\langle 34\bar{7}3 \rangle$. This agreement is fortuitous but the use of $D_L = 7.9 \times 10^{-6}$ cm^2 s^{-1} (see Section VI) gives $\delta = 0.16$ mm which is probably correct to the order of magnitude.

Attempts to detect a solute boundary layer of high Co concentration ahead of the interface were unsuccessful as would be expected if $\delta \stackrel{\sim}{<} 1$ mm. The width of the laser beam as it passes through the sample is 1-2 mm so changes in concentation over smaller distances than this are not detectable. Scans of absorption versus position in the liquid at various stages of growth were analyzed in an attempt to detect variations with time which would indicate slow convection, but no systematic charges could be seen and all our evidence suggests that mixing is rapid, presumably because of lateral temperature gradients.

VI. DISTRIBUTION COEFFICIENT IN CZOCHRALSKI GROWTH

Crystal growth by pulling from the melt allows the determination of k both by varying the pull rate V and the rotation rate ω which determines the thickness of the boundary layer δ.

Examples of crystals grown by pulling from the melt are shown in Fig. 15. The largest crystals grown were pulled from crucibles 4.2 cm in internal diameter and in height and were up to 2.2 cm in diameter and 100g in weight. Larger crystals could presumably be grown without difficulty by scaling up the apparatus.

It is necessary to prevent thermal shock in order to avoid cracks and thus the pulled crystals were cooled very slowly and then annealed at 300°C prior to fabrication. All the crystals have round shapes and no prominent facets.

Three prominent directions were chosen to grow $CsCdCl_3$, which are [0001], [10$\bar{1}$0], and [10$\bar{1}$2]. We have not had any major problems in growing it along any particular direction. For comparison, the [0001] and [10$\bar{1}$0] directions were chosen for this study of solute redistribution. To observe the solute distribution change due to the velocity change effect only, the crystal diameter must be small enough not to be affected by any crucible wall effect; i.e., the melt is perfectly mixed by crystal rotation and solute convection in the melt near the crystal interface is not significantly influenced by the crucible wall. A rotation rate of 15 rpm was used for all crystals grown at different values of V, up to a maximum of 4 cm/s. The weight was between 5g and 10g from a total charge weight of 50g.

When crystals were grown at varying ω (fixed V), problems were encountered because of the change in diameter caused by changing convective
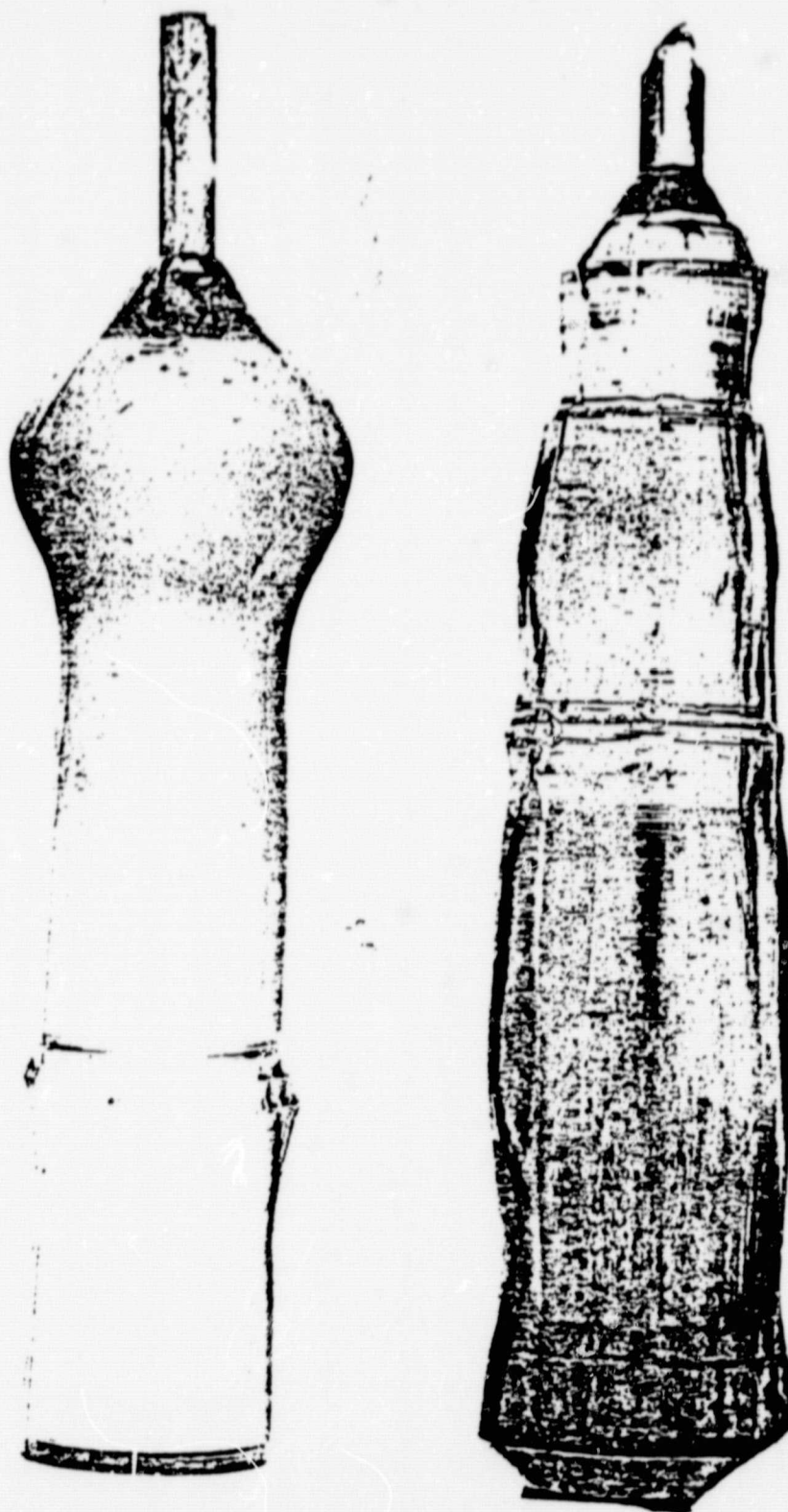
Figure 15: Crystals of $CsCdCl_3$ grown by pulling from the melt;

Left: Undoped crystal grown in [0001] direction;
Right: Co-doped crystal grown in [10$\bar{1}$0]. Both are roughly 2 cm in diameter and 10 cm long.

flow as the crystal rotation rate was varied. To study the rotation rate change effects on solute redistribution, we used rates from 2.2 rpm to 100 rpm. At 120 rpm, the crystal exhibited an irregular cross-section.

The cobalt concentration C_S was measured by polishing the crystal along opposite sides and measuring the absorption of the He-Ne laser beam. The absorption was calibrated against samples analyzed by spark s. ce emission spectroscopy which had been found to be accurate within ± 10%. The calibration gives the concentation in ppm as 220.4 α where α is the measured absorption coefficient.

Data for <0001> and <10$\bar{1}$0> orientations are shown in Figs. 16 and 17. The slope of Fig. 17 is 1.6 $\nu^{1/6} V^{3/2} D_L^{-1}$ [3] so that D_L can be evaluated using data for the kinematic viscosity ν from Table 1. From the average slopes we obtain $D_L = 8.38 \times 10^{-6}$ cm^2 s^{-1} from the <0001> data and $D_L = 7.43 \times 10^{-6}$ cm^2 s^{-1} for <1010> so the two values are in good agreement.

To determine the values $\beta_S/\tilde{k}T$ and α_S for each orientation, we use the two sets of equations $d/dV \, [\ln(1/k-1)]_{<0001>} = -2396$ sec/cm and $\ln((\tilde{\gamma}_S+1)/k_o')_{<0001>} = 1.92$ for the <0001> orientation plus $d/dV \, [\ln(1/k-1)]_{<10\bar{1}0>} = -1832$ sec/cm and $\ln((\tilde{\gamma}_S+1)/k_o')_{<10\bar{1}0>} = 2.03$ for the <10$\bar{1}$0> orientation, all at $V = 0.6$ cm/hr. However, we do not have enough data to find the independent D_S value so we must use $\alpha_S D_S$ as a single value. Therefore, for the <0001> orientation
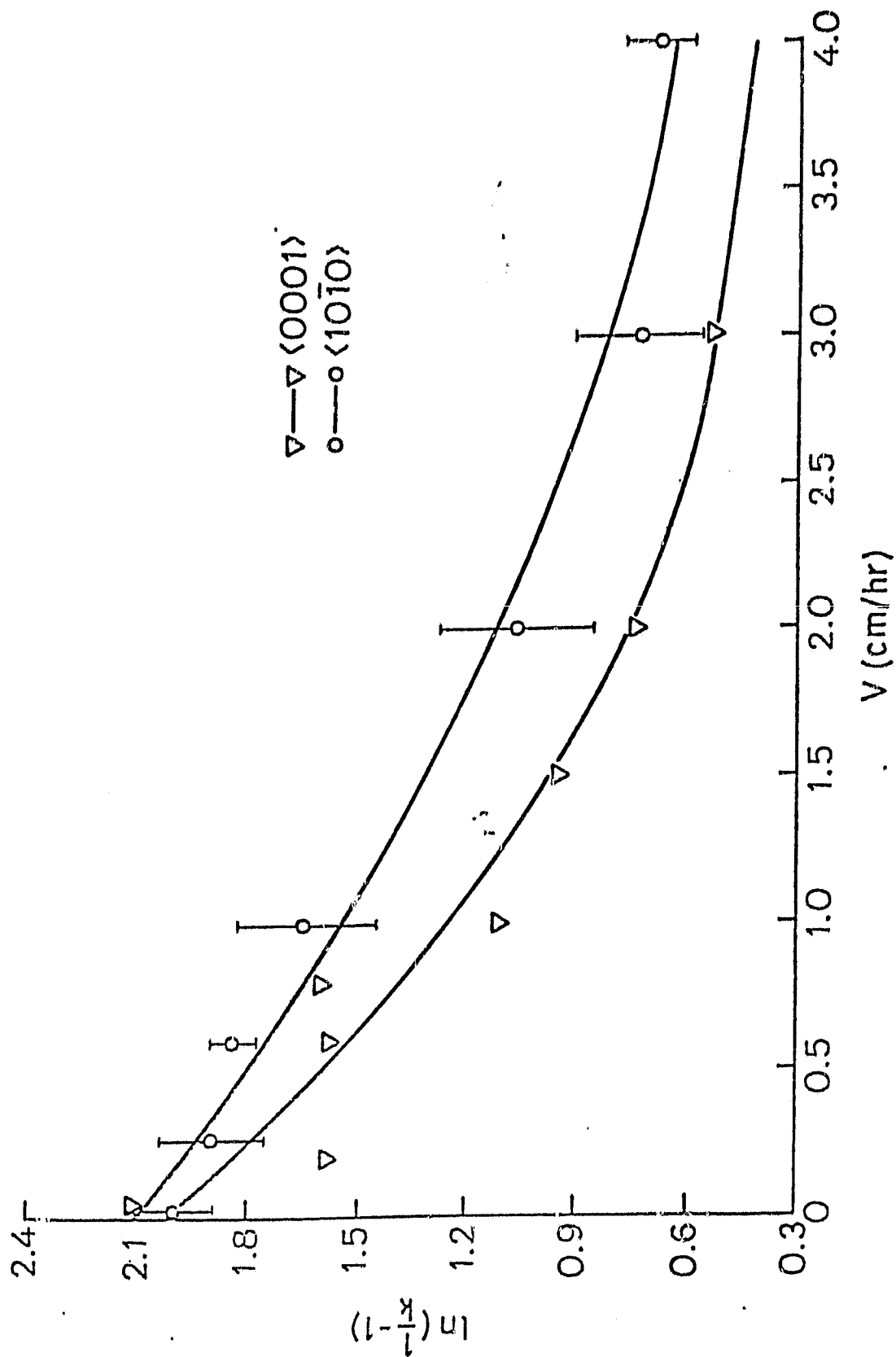
Figure 16: Measured plots of $\ln(1/k - 1)$ versus V for the Co – CsCdCl$_3$ system
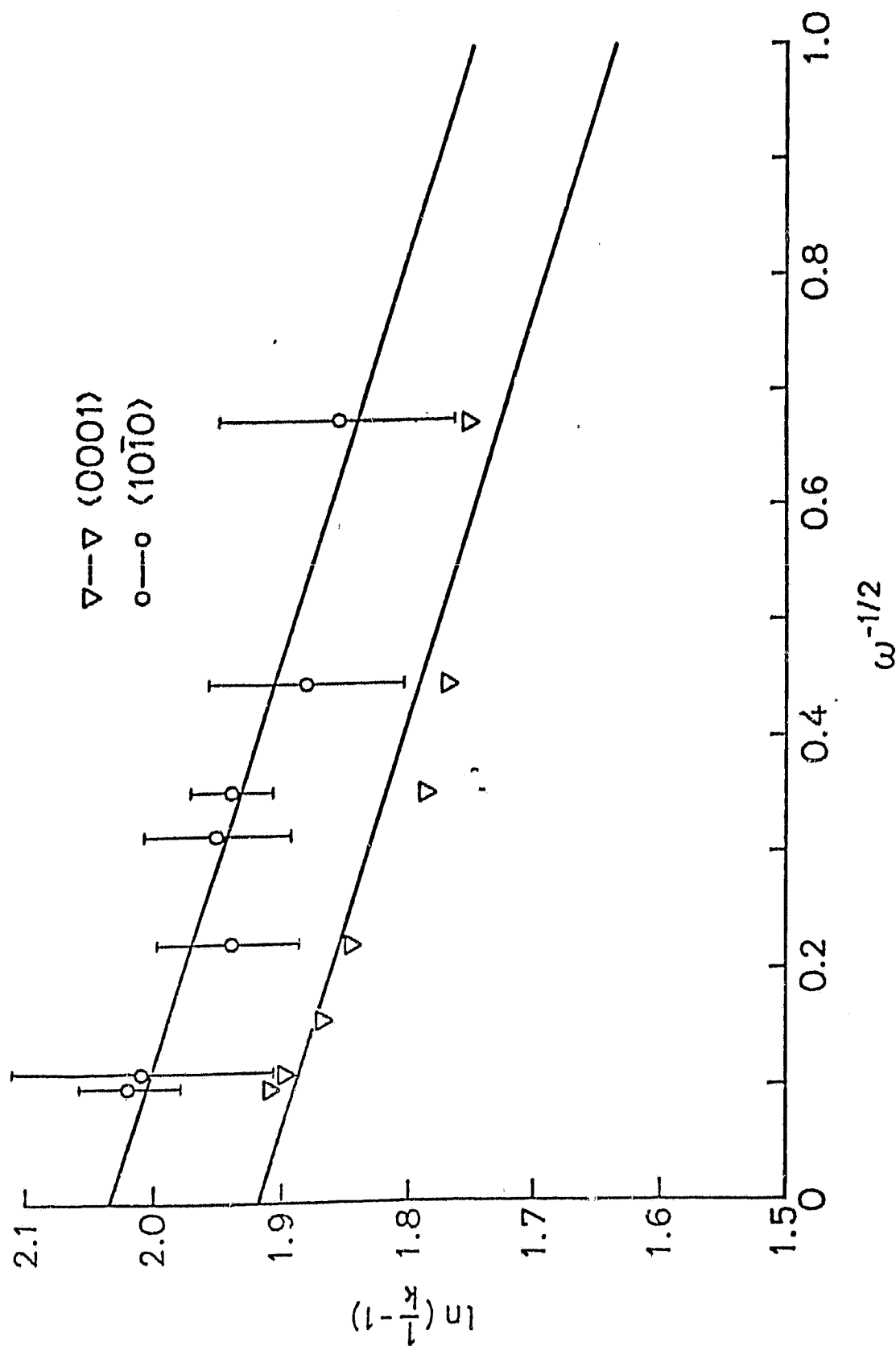
Figure 17: Measured plots of $\ln(1/k - 1)$ versus $\omega^{-1/2}$ for the Co-CsCdCl$_3$ system

$$\frac{1}{1 + \tilde{\gamma}_S - k'_o} \sum_{n=1}^{\infty} \frac{(\beta_S/\tilde{kT})^n}{\alpha_S Dn \; n!} \approx 1.734 \times 10^3 \; ,$$

and

$$\tilde{\gamma}_S = \sum_{n=1}^{\infty} \frac{(\beta_S/\tilde{kT})^n}{(1 + \frac{\alpha_S D_S n}{V}) \; n!} = -0.1006 \; ,$$

while, for the $\langle 10\bar{1}0 \rangle$ orientation,

$$\frac{1}{1 + \tilde{\gamma}_S - k'_o} \sum_{n=1}^{\infty} \frac{(\beta_S/\tilde{kT})^n}{\alpha_S Dn \; n!} \approx 1.377 \times 10^3 \; ,$$

$$\tilde{\gamma}_S = \sum_{n=1}^{\infty} \frac{(\beta_S/\tilde{kT})^n}{(1 + \frac{\alpha_S D_S n}{V}) \; n!} = -0.0094 \; .$$

From these we can deduce the following results:

- $\langle 0001 \rangle$ orientation

$$\frac{\beta_{S\langle 0001 \rangle}}{\tilde{kT}} = -1.50 \; , \quad \alpha_{S\langle 0001 \rangle} \cdot D_S = 1.58 \times 10^{-3}$$

- $\langle 10\bar{1}0 \rangle$ orientation

$$\frac{\beta_{S\langle 10\bar{1}0 \rangle}}{\tilde{kT}} = -1.25 \; , \quad \alpha_{S\langle 10\bar{1}0 \rangle} \cdot D_S = 3.98 \times 10^{-3} \; .$$

From the above result, we know that the {0001} have the larger interface field strength which is what one might have expected bacause the {0001} are the close packed planes in $CsCdCl_3$ (H.C.P. structure). A summary of these determined properties is given in Table 3.

It should be noted that distribution coefficient data for the same orientation are very different according to whether crystals are grown by gradient freezing or pulling from the melt. A direct comparison is shown in Fig. 18. The slopes are, by coincidence, very similar but what is striking is the large difference in intercept. In this case, with the data fitted in each case by a straight line chosen by the least squares method, the intercepts are $k_{V=0} = .027$ for gradient freeze method and $k_{V=0} = 0.136$ for pulling from the melt. It is clear that the intercept cannot be the equilibrium value in both cases. An interpretation based on the interface field concept gives the intercept as $(1+\gamma_S)/k_o'$ with γ_S an incomplete gamma function and $k_o' \sim k_o[\gamma_S(\infty)/\gamma_S(0)]^C$. Given that the distribution of solute ahead of the interface is different in the two cases, we might expect differences in the interface field to account for some of the discrepancy between the two intercepts. It is still doubtful, however, whether we can account for a factor of 5 when the system and orientation are the same.

This large difference between the two sets of data is clearly an important result which shows that a single set of distribution coefficient data cannot be relied upon to give the equilibrium value. Any detailed interpretation is still speculative at the present time.

Table 3

Summary of Physical Properties of $CSCd_{0.99}Co_{0.01}Cl_3$

$$D_L = (7.91 \pm 0.48) \times 10^{-6} \ cm^2/sec$$

$$k_O' = 0.115$$

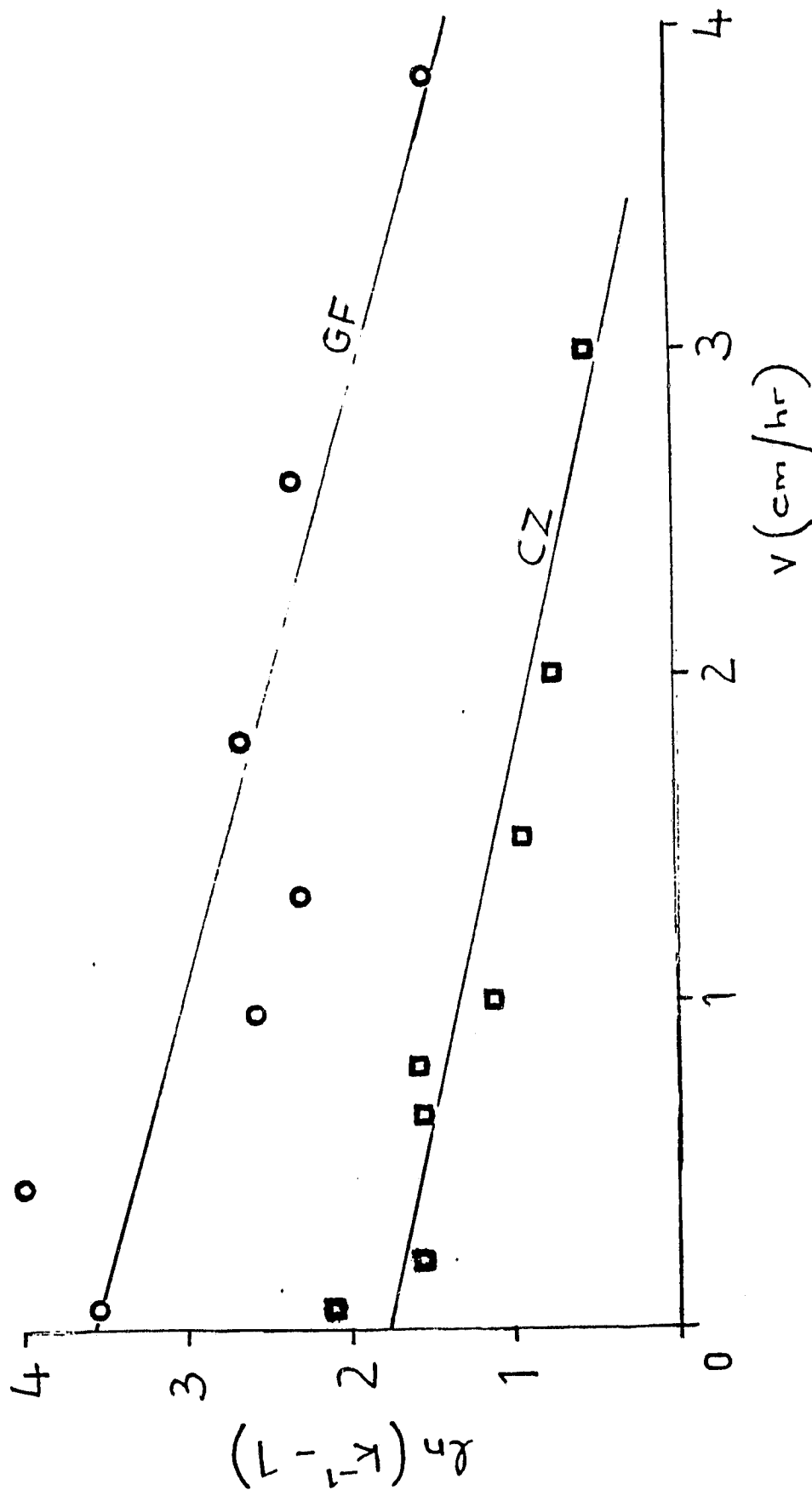|	<0001>	<1010>
$\tilde{\beta}_S/kT$	-1.50	-0.25
$\alpha_S D_S$	1.58×10^{-3} cm/sec	3.98×10^{-3} cm/sec

Figure 18: Log of ($k^{-1} - 1$) versus growth rate V for cobalt in $CsCdCl_3$; GF=gradient freeze; CZ=Czochralski method

VII. SUMMARY AND CONCLUSIONS

1. The introduction of an interface field term due to local atomic
configurations at the solid-liquid interface has been shown to have a
significant influence on the theory of solute distribution. This
effect can explain the observed curvature in the $\ln(k^{-1}-1)$ versus
growth rate data for germanium.

2. The interface field effect has been introduced into the constitutional
supercooling and morphological stability theories. Both stabilizing
and destabilizing effects may result, and the magnitude of the
resulting changes can be several orders of magnitude.

3. A new model material for crystal growth studies, $CsCdCl_3$, has been
grown by both gradient freeze and Czochralski methods. Cobalt-doped
melts in particular are very attractive for direct observational
studies at temperatures where the infra-red radiation background is
negligible.

4. Studies of interface shape and the breakdown of stable growth have
revealed a sensitivity of the interface curvature to the cobalt
concentration in the liquid. This effect, attributed to radiation
absorption in the liquid, has been neglected in previous studies of
this kind.

5. A new technique for measurement of distribution coefficient by laser
light absorption has been developed.

6. Distribution coefficients during gradient freeze growth were found to
    be systamtically lower than those for Czochralski growth over the same
    range of growth rates. The values for the <0001> direction
    extrapolated to $V = 0$ differed by a factor 5, indicating a large
    difference from equilibrium in one or both cases.

REFERENCES

[1] W.A. Tiller and K.S. Ahn, J. Crystal Growth, 49 (1980), 483.

[2] K.S. Ahn, Ph.D. Thesis, Stanford University, 1981.

[3] J.A. Burton, R.C. Prim and W.P. Slichter, J. Chem. Phys., 21 (1953), 1987.

[4] R.N. Hall, Phys. Rev. 88 (1952), 139.

[5] F.A. Trumbore, Bell System Tech. J., 39 (1960), 205.

[6] N.B. Hannay, Semiconductors (Reinhold, London, 1959), p. 244.

[7] K.S. Ahn and W.A. Tiller, to be published.

[8] W.W. Mullins and R.F. Sekerka, J. Appl. Phys., 35 (1964), 444.

[9] V.V. Voronkov, Sov. Phys. Sol. St., 6 (1965), 2378.

[10] G.R. Kotler, Stanford University Ph.D. Thesis, 1967.

[11] R. Trivedi and W.A. Tiller, Acta. Met., 26 (1978), 671.

[12] K.S. Ahn, R.A. Carranza, D. Elwell, and R.S. Feigelson, J. Cryst. Growth, 50 (1980), 775.

[13] I.N. Belyaev, D.S. Lesnykh, A.K. Doroshenko, and E.G. Eikenbaum, Zh. Prikl. Khim., 45 (1972), 665.

[14] S. Siegel and E. Gebert, Acta Cryst., 17 (1964), 790.

[15] S. V. Naray-Szabo, Structure Repts., 11 (1947-48), 454.

[16] K.J. Marsh and J.A. Savage, J. Mater. Sci., 14 (1979), 2157.

[17] R.H. Geils and R.C. Keezer, Rev. Sci. Instrum, 48 (1977), 783.

[18] R.S. Feigelson and R.K. Route, J. Crystal Growth, 49 (1980), 261.

[19] C.E. Chang and W.R. Wilcox, J. Crystal Growth, 21 (1974), 135.